Density of conjugated antibody determines the extent of Fc receptor dependent capture of nanoparticles by liver sinusoidal endothelial cells

Kappel, C.; Seidl, C.; Medina-Montano, C.; Schinnerer, M.; Alberg, I.; Leps, C.; ... ; Grabbe, S.

ACSNANO

www.acsnano.org

ARTICLE

Density of Conjugated Antibody Determines the Extent of Fc Receptor Dependent Capture of Nanoparticles by Liver Sinusoidal Endothelial Cells

Cinja Kappel, Christine Seidl, Carolina Medina-Montano, Meike Schinnerer, Irina Alberg, Christian Leps, Julian Sohl, Ann-Kathrin Hartmann, Michael Fichter, Michael Kuske, Jenny Schunke, Gabor Kuhn, Ingrid Tubbe, David Paßlick, Dominika Hobernik, Rebekka Bent, Katharina Haas, Evelyn Montermann, Kerstin Walzer, Mustafa Diken, Manfred Schmidt, Rudolf Zentel, Lutz Nuhn, Hansjörg Schild, Stefan Tenzer, Volker Mailänder, Matthias Barz,* Matthias Bros,* and Stephan Grabbe*

Cite This: *ACS Nano* 2021, 15, 15191−15209

Read Online

ACCESS | Metrics & More | Article Recommendations | Supporting Information

ABSTRACT: **Despite considerable progress in the design of multifunctionalized nanoparticles (NPs) that selectively target specific cell types, their systemic application often results in unwanted liver accumulation. The exact mechanisms for this general observation are still unclear. Here we asked whether the number of cell-targeting antibodies per NP determines the extent of NP liver accumulation and also addressed the mechanisms by which antibody-coated NPs are retained in the liver. We used polysarcosine-based peptobrushes (PBs), which in an unmodified form remain in the circulation for >24 h due to the absence of a protein corona formation and low unspecific cell binding, and conjugated them with specific average numbers (2, 6, and 12) of antibodies specific for the dendritic cell (DC) surface receptor, DEC205. We assessed the time-dependent biodistribution of PB−antibody conjugates by *in vivo* imaging and flow cytometry. We observed that PB−antibody conjugates were trapped in the liver and that the extent of liver accumulation strongly increased with the number of attached antibodies. PB−antibody conjugates were selectively captured in the liver *via* Fc receptors (FcR) on liver sinusoidal endothelial cells, since systemic administration of FcR-blocking agents or the use of $F(ab')_2$ fragments prevented liver accumulation. Cumulatively, our study demonstrates that liver endothelial cells play a yet scarcely acknowledged role in liver entrapment of antibody-coated NPs and that low antibody numbers on NPs and the use of $F(ab')_2$ antibody fragments are both sufficient for cell type-specific targeting of secondary lymphoid organs and necessary to minimize unwanted liver accumulation.**

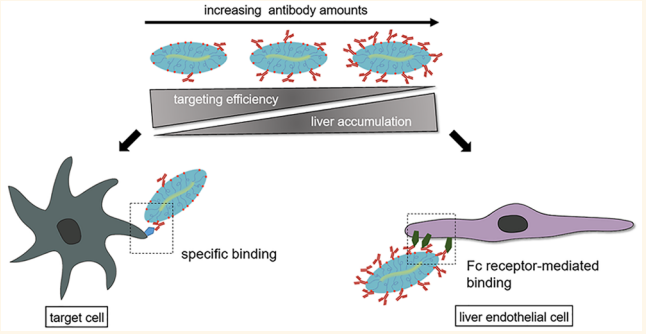

KEYWORDS: *nanoparticle, antibody, targeting, biodistribution, liver accumulation, liver endothelial cells, polypept(o)ides*

INTRODUCTION

During the last 40 years, nanoparticles (NPs) have evolved as carrier systems for tissue- and cell type-directed drug delivery to reduce adverse effects of active pharmaceutical ingredients.[1] However, the efficacy at which systemically applied NPs deliver drugs to specific cell types *in vivo* is still far from optimal.[2] The first generation of NPs developed for tumor targeting, *e.g.*, Doxil, exploited passive accumulation within solid tumors by the enhanced permeability and retention (EPR) effect.[3] More recently, NP-mediated targeting of immune cells in order to induce immunity against tumors[4] or pathogens[5] has attracted increasing interest,[6] since immune cells within blood or lymphoid organs are more easily

Received: July 6, 2021
Accepted: August 3, 2021
Published: August 25, 2021

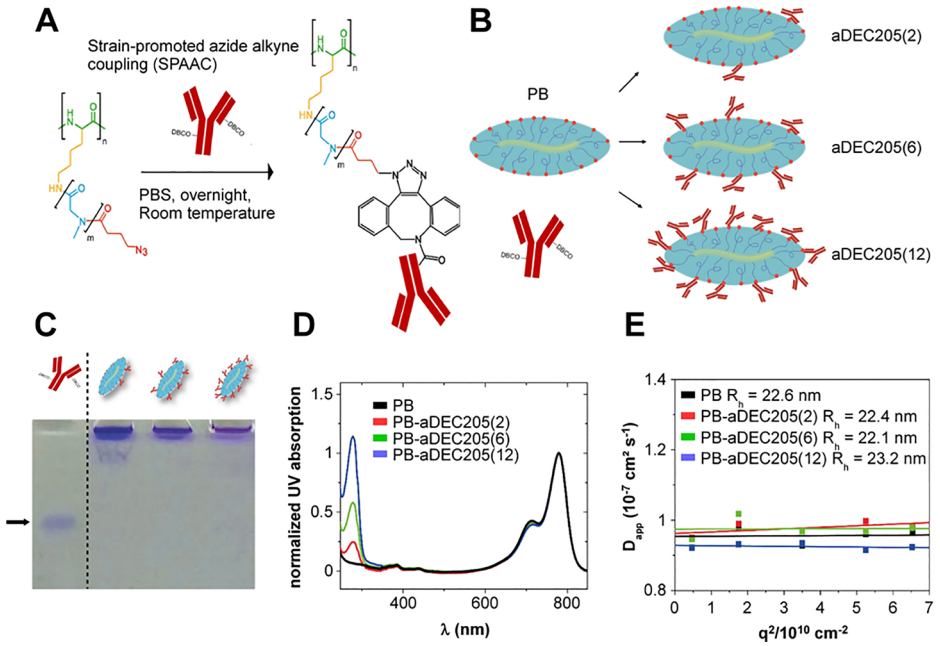

Figure 1. Synthesis and characterization of PB−antibody conjugates: (A) Scheme of strain-promoted azide−alkyne cycloaddition (SPAAC) reaction employed for antibody conjugation; (B) schematic illustration of PB−aDEC205 antibody conjugates; (C) SDS-PAGE electrophoresis to control for contaminating free Ab within the PB conjugates (lane 1: nonconjugated aDEC205 antibody (band indicated by arrow), lanes 2−4 PB−aDEC205 antibody conjugates); (D) UV−vis analysis of the effectivity of antibody conjugation; (E) multiangle DLS analysis of PB−aDEC205 antibody conjugates.

accessible by systemically applied NPs.[7] Myeloid cells, such as macrophages (Mphs) and dendritic cells (DCs), that are specialized to recognize nanosized pathogens[8] were shown to internalize synthetic NPs spontaneously and after complement- or immunoglobulin-mediated opsonisation.[9,10] Mphs degrade and internalize material more efficiently than DCs, whereas DCs potently process pathogen-derived antigens and present them to T cells as a necessary step to induce antigen-specific T cell responses for induction of immunity or tolerance.[11] Therefore, the design of NPs that actively target DCs to minimize unwanted binding/uptake by Mphs and other cell types with endocytic and phagocytic capacity is in the focus of research.[12]

Antibodies are the most widely used tools to selectively target NPs to certain cell types such as DCs. The attachment of several antibodies per NP increases the overall avidity, which may result in enhanced NP binding and uptake, suggesting that an increase in valency of targeting moieties may be a desirable goal of NP design.[13] However, it was also reported that lowered avidity can increase selectivity of cell-targeting NPs.[4] Commonly applied antibody conjugation strategies result in a nonoriented attachment of the antibody to the NP, where the constant Fc (fragment crystallizable) part may be exposed and can facilitate unwanted binding to Fc receptors (FcRs) that are widely expressed in the body.[15] Thus, novel strategies to minimize capture of NPs by nontarget cells are needed to improve target cell selectivity requires a more detailed understanding of underlying effects.[16] To assess cell-specific targeting, NPs that exert minimal unspecific binding and thus elongated plasma circulation times of 24 h and seem beneficial,[10] which continues to be a significant methodological problem. Moreover, it has been a synthetic challenge to generate NPs with a defined (average) antibody number[17] in a reproducible and scalable manner.[18] Thus, comparative studies on the biodistribution of antibody-decorated NPs so far mainly focused either on NP accumulation in distinct organs[19] or on target cell type-specific binding.[20]

Therefore, our study aimed to delineate the role of antibody number on stealth-like NPs for their biodistribution at organ and single-cell levels, the specificity of cell type targeting, and the mechanisms by which nontargeted cell types may compete for NP engagement. To this end, we employed polysarcosine-based cylindrical polymer brushes[21] with a circulation half-life of >24 h, due to the stealth-like nature of polysarcosine[22] that results in very low interaction with plasma proteins and cells *in vivo*.[23,24] NPs were conjugated with distinct average numbers of antibodies, namely, 2, 6, and 12, targeting the surface receptor DEC205 (CD205), a type I cell surface protein predominantly expressed by DCs.[25] Using these antibody-coated peptobrushes, we analyzed their biodistribution by *in vivo* and *ex vivo* imaging and flow cytometry of liver, spleen, and lymph node (LN) cells, generating detailed insight on organ and cellular distributions of NPs in relation to the number of antibodies attached to their surface.

RESULTS AND DISCUSSION

Polysarcosine-Based Peptobrushes Can Be Precisely Functionalized with Defined Numbers of Antibodies. For synthesis of the polysarcosine-based cylindrical brush polymers, termed peptobrushes (PBs),[26] the backbone $pLys_{250}$ was used as a macroinitiator for the controlled living ring-opening polymerization of sarcosine *N*-carboxy anhydride yielding polysarcosine side chains (Figure 1A). End group functionalization was performed by azido-butyric acid pentafluorophenylester to obtain a quantitative azide functionality allowing antibody conjugation by azide−alkyne coupling. The polysarcosine side chains provide a high biocompatibility and enzymatic and oxidative biodegradability of the PBs.[27]

https://doi.org/10.1021/acsnano.1c05713
ACS Nano 2021, 15, 15191−15209

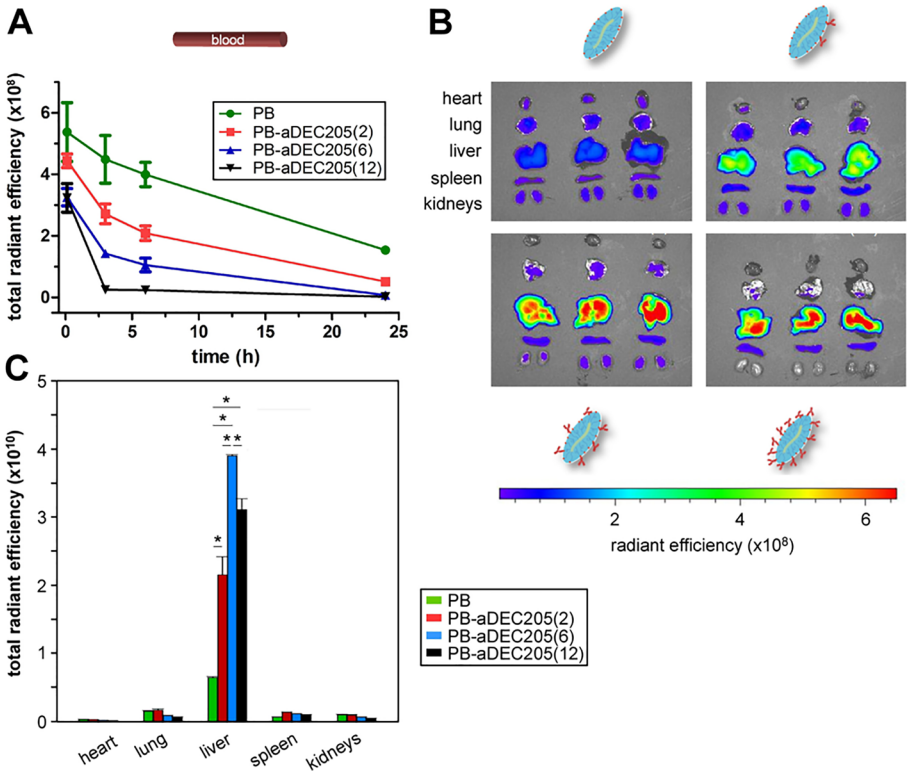

Figure 2. The extent of liver accumulation of systemically applied PB−antibody conjugates correlates with antibody density: (A−C) CW800-labeled PBs were systemically injected into mice. (A) Blood was retrieved at the time points indicated, and contents of PBs were quantified by measurement of fluorescence intensities. Data indicate the mean ± SEM of 3 samples per group and time point. (B) Fluorescence imaging of organs retrieved from mice treated with the various PBs at 24 hpi. (C) Quantification of organ-specific CW800 fluorescence (see B). Data denote the mean ± SEM of 6−8 samples per group (compiled from 2 to 3 experiments; one-way ANOVA, significance: *$p < 0.05$).

Furthermore, PBs of different sizes were shown to display long circulation half-lives of up to 7 days in zebrafish larvae.[28]

CD8α^+ conventional type 1 DCs (cDC1) are characterized by expression of the C-type lectin receptor DEC205 (CD205) and are capable of cross-presenting exogenous antigens *via* MHC-I to CD8$^+$ T cells.[29] We and others have previously shown that antigen targeted to DEC205 by specific antibodies results in endocytic uptake by DCs and efficient antigen presentation.[20,25] Therefore, to address DCs as a suitable target cell type for nanovaccines, we used an anti-DEC205 antibody (aDEC205) for conjugation with PBs. aDEC205 was modified with a DBCO linker to allow for chemoselective bioconjugation to azide groups on the peptobrush by strain-promoted azide−alkyne cycloaddition (SPAAC), a well-established protocol for the attachment of antibodies to nanoparticles.[30] The antibody retained its binding affinity toward DCs whenever fewer than three DBCO molecules on average were bound to the antibody. The conjugation to the brush, however, results in a more or less random manner since the reactive ester reacts with the primary amine of lysines within the antibody. As a consequence of this nondirective antibody conjugation to the NP surface, some of the NP-bound antibodies likely have an outward orientation of their Fc region, which may enable FcR-mediated binding. Since antibody conjugation is performed according to established protocols at physiological temperature and pH, the structural integrity of the antibody is maintained. Moreover, purely by stoichiometry a distinct average number of antibodies, namely, 2, 6, and 12, can be conjugated to PBs (Figure 1B). SDS-PAGE electrophoresis revealed complete conjugation of introduced antibodies (Figure 1C). UV−vis spectroscopy confirmed conjugation of the desired numbers of antibodies per PB (Figure 1D). Multiangle dynamic light scattering (DLS) analysis demonstrated similar sizes of all PB−antibody conjugates (Figure 1E). For detection of the PBs in subsequent analysis the near-infrared dye CW800 was conjugated by SPAAC.

The Antibody Number of PB Correlates with Their Accumulation in the Liver and Inversely Correlates with Their Blood Circulation Time. We used PB−antibody conjugates with the three different antibody numbers to investigate the impact of increasing antibody density per PB on their pharmacokinetics and biodistribution after intravenous injection. For this, *in vivo* imaging was combined with *ex vivo* analysis of blood and internal organs. As expected, PB without antibody displayed the longest half-life in blood (Figure 2A). All PB−antibody conjugates exhibited reduced blood circulation times, which inversely correlated with the number of attached antibodies. This effect was most pronounced in the case of PB conjugated with the highest number of antibodies (PB−aDEC205[12]). In accordance with the stealth-like properties, polysarcosine PB polymers without conjugated antibodies were scarcely detectable in any of the monitored internal organs at 24 h postinjection (hpi) (Figure 2B,C). In contrast, all PB−antibody conjugates could be found in the liver. The extent of liver deposition was lowest in the case of PB conjugated with two antibodies (PB−aDEC205[2]), whereas PB with intermediate (PB−aDEC205[6]) and high (PB−aDEC205[12]) antibody numbers per brush accumulated at higher extents (almost 2-fold for PB−aDEC205[12]).

https://doi.org/10.1021/acsnano.1c05713
ACS Nano 2021, 15, 15191−15209

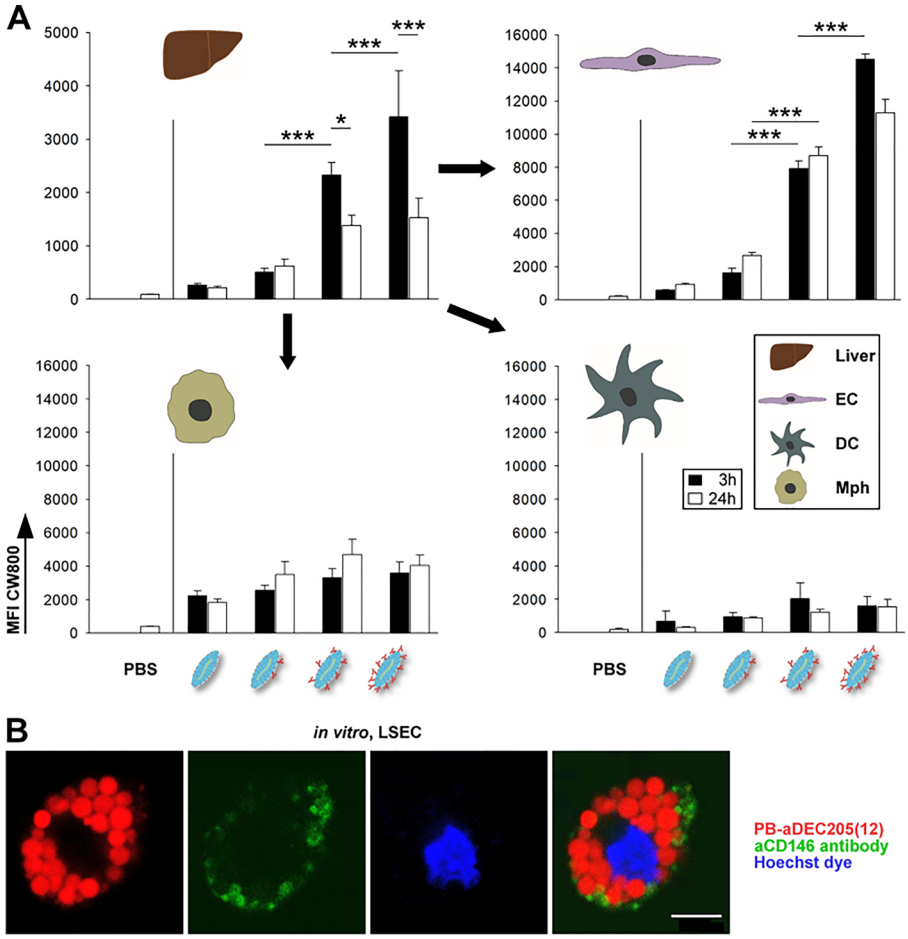

Figure 3. In the liver PB−antibody conjugates engage predominantly endothelial cells, in correlation with PB antibody number: (A) Flow cytometric analyses of liver non-parenchymal cell (NPC) populations at various time points after systemic application of different PB conjugates (black bars: 3 hpi, white bars: 24 hpi). Liver NPCs of mice differentially treated with CW800-labeled PBs were prepared and incubated with antibodies to differentiate liver endothelial cells (ECs: $CD45^{-}CD31^{+}$), macrophages (Mphs: $CD45^{+}F4/80^{+}$), and dendritic cells (DCs: $CD45^{+}CD11c^{+}$). Upper left panel: total liver NPCs, upper right panel: liver endothelial cells, lower left panel: liver Mphs, lower right panel: liver DCs. Data denote the CW800 mean fluorescence intensities (MFI) of either NPC population (mean ± SEM, $n = 6-8$ obtained from 2 to 3 experiments; one-way ANOVA, $*p < 0.05$, $***p < 0.001$). (B) Confocal laser scanning microscopy image of a liver endothelial cell incubated with PB−aDEC205(12) conjugate for 1 h *in vitro*. Cells were incubated with anti-CD146 antibodies to identify liver sinusoidal endothelial cells (LSECs: $CD45^{-}CD31^{+}CD146^{+}$) and Hoechst dye for nuclear staining. Scale bar: 10 μm.

A similar biodistribution pattern was observed also at 3 hpi (see Figure 4C, upper panel) and in Figure 4D.

To elucidate which cell populations within the liver engaged the various PBs, liver cell suspensions were subjected to flow cytometric analysis. Here we focused on non-parenchymal cell (NPC) types previously shown to interact with different types of NPs.[31,32] In accordance with the imaging results, we observed that the mean fluorescence intensity (MFI) of total liver NPCs increased in correlation with PB antibody density at 3 hpi as well as 24 hpi (Figure 3A, upper left panel).

Further analysis of distinct liver NPC populations revealed that PBs with intermediate/high antibody numbers were largely associated with liver endothelial cells (ECs) (Figure 3A, upper right panel). Again, the extent of EC engagement correlated with the number of antibodies per PB. On the contrary, the number of antibodies per PB had no major effect on engagement by $F4/80^{+}$ liver Mphs, which may be largely attributed to Kupffer cells that constitute >80% of liver Mphs,[33,34] and DCs, as measured by MFI, which correlates to the number of NPs per cell (Figure 3A) in the applied concentration range. In agreement, at 3 hpi the numbers of PB-positive liver NPCs and ECs correlated with the number of antibodies per PB, in contrast to Mphs and DCs (see Supp Figure 1).

Within the liver EC population, $CD146^{+}$ liver sinusoidal endothelial cells (LSECs) have been reported to engulf NPs.[19] Therefore, we assessed whether antibody-coated PBs were indeed internalized by these cells. As depicted in Figure 3B, PB−aDEC205(12) were readily internalized *in vitro* by $CD146^{+}$ LSECs after co-incubation for 1 h and accumulated in discrete intracellular vesicle-like structures.

Altogether, these findings indicate that PBs with low antibody numbers per PB exhibit only limited undesired liver accumulation, whereas an intermediate antibody density was sufficient to confer massive deposition of PB-based NPs in the liver. Surprisingly, liver ECs exerted a stronger PB−antibody conjugate binding capacity than Mphs (and DCs), in terms of both numbers of PB-engulfing cells and the number of PBs engaged per cell (MFI).

Liver ECs Engage PB−Antibody Conjugates *via* Fcγ Receptors. LSECs have been demonstrated to play an important immunological role by internalizing immune

https://doi.org/10.1021/acsnano.1c05713
ACS Nano 2021, 15, 15191−15209

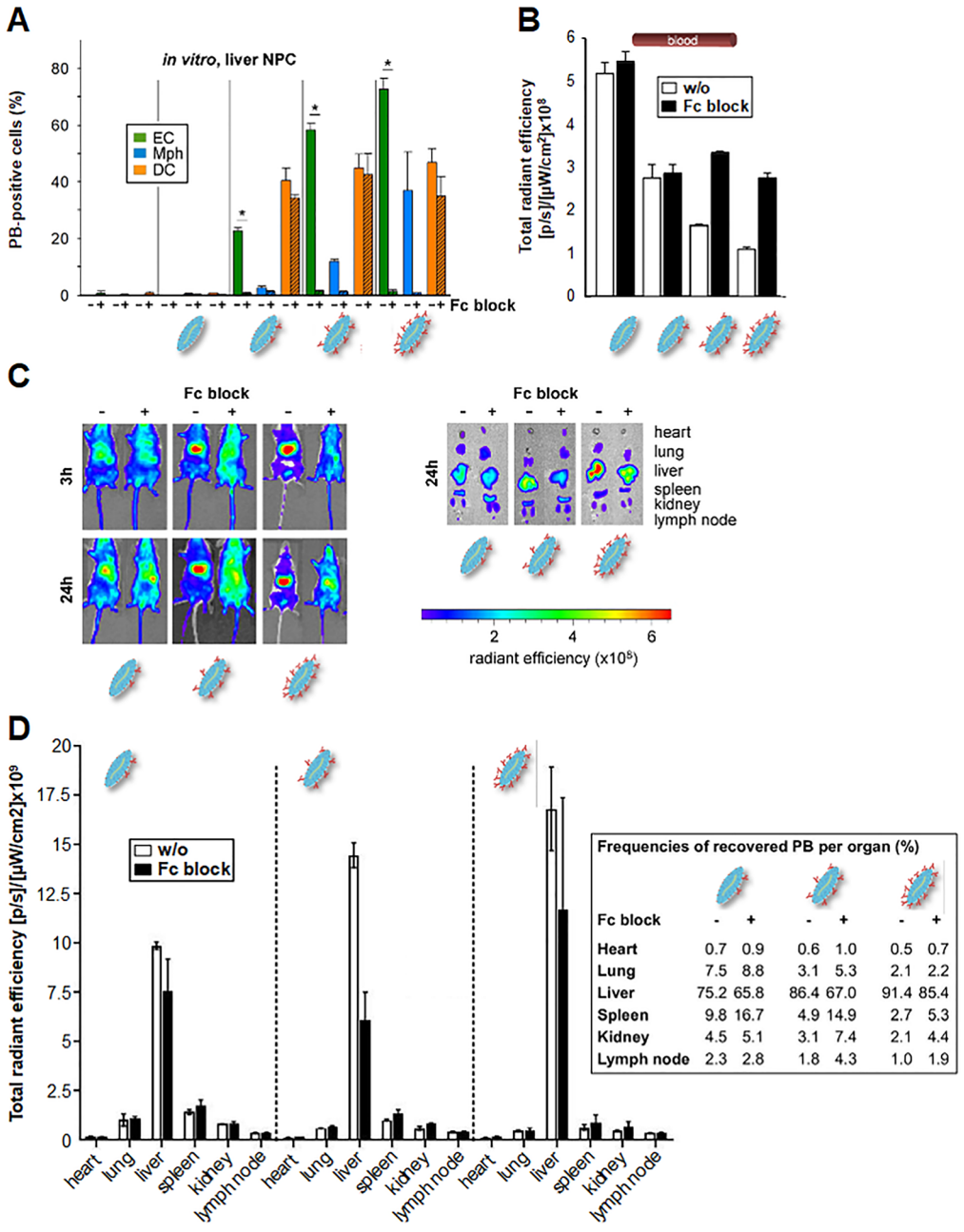

Figure 4. Systemic blockade of Fc receptors reduces liver accumulation of PB–antibody conjugates with intermediate and high antibody density: (A) Isolated liver NPCs (liver endothelial cells (ECs: CD45$^-$CD31$^+$), macrophages (Mphs: CD45$^+$F4/80$^+$), and dendritic cells (DCs: CD45$^+$CD11c$^+$)) were preincubated with an FcγRII/III-blocking antibody (Fc block), followed by incubation with PB conjugates for 1 h. Data denote the frequencies of PB-positive cells of the different NPC populations as assessed by flow cytometry (see legend of Figure 3A) and represent the mean ± SEM (n = 3; one-way ANOVA, *p < 0.001). (B–D) Mice were pretreated with Fc block, followed by systemic application of PB conjugates. (B) Blood was retrieved 6 hpi, and contents of PBs derived from mice left untreated (w/o) or after pretreatment with Fc block were quantified (mean ± SD, n = 2 per group). (C) Fluorescence imaging of mice at 3 and 24 hpi (left panel) and of organs retrieved 24 hpi (right panel). (D) Quantification of organ-specific fluorescence at 24 hpi (see C, right panel). Data denote the mean ± SD of 2 samples per group (one-way ANOVA, significance: *p < 0.001). Data in the table depict the relative percentage of recovered fluorescence per organ (fluorescence of all organs combined = 100%).

complexes *via* different types of surface receptors including the Fcγ receptor IIb (FcγRIIb),[35] which is not expressed by other hepatic EC populations and is largely confined to immune cells.[36] Since aDEC205 antibodies were conjugated to PBs in a more or less random manner, the Fc part of a fraction of these may be accessible for binding. We tested the potential role of the Fc/FcγRIIb interaction for the observed binding and uptake of PB–antibody conjugates by liver ECs in blocking studies. To this end, isolated primary liver NPCs were preincubated with anti-FcγRIIb/FcγRIII-specific antibodies known to block Fc-mediated binding and subsequently incubated with the different PB conjugates. PB without antibody showed no cellular interaction at the applied concentration (10^{12} particles per mL on 10^6 cells). As observed before, the frequencies of ECs and Mphs that engaged PB–antibody conjugates correlated with increasing

https://doi.org/10.1021/acsnano.1c05713
ACS Nano 2021, 15, 15191–15209

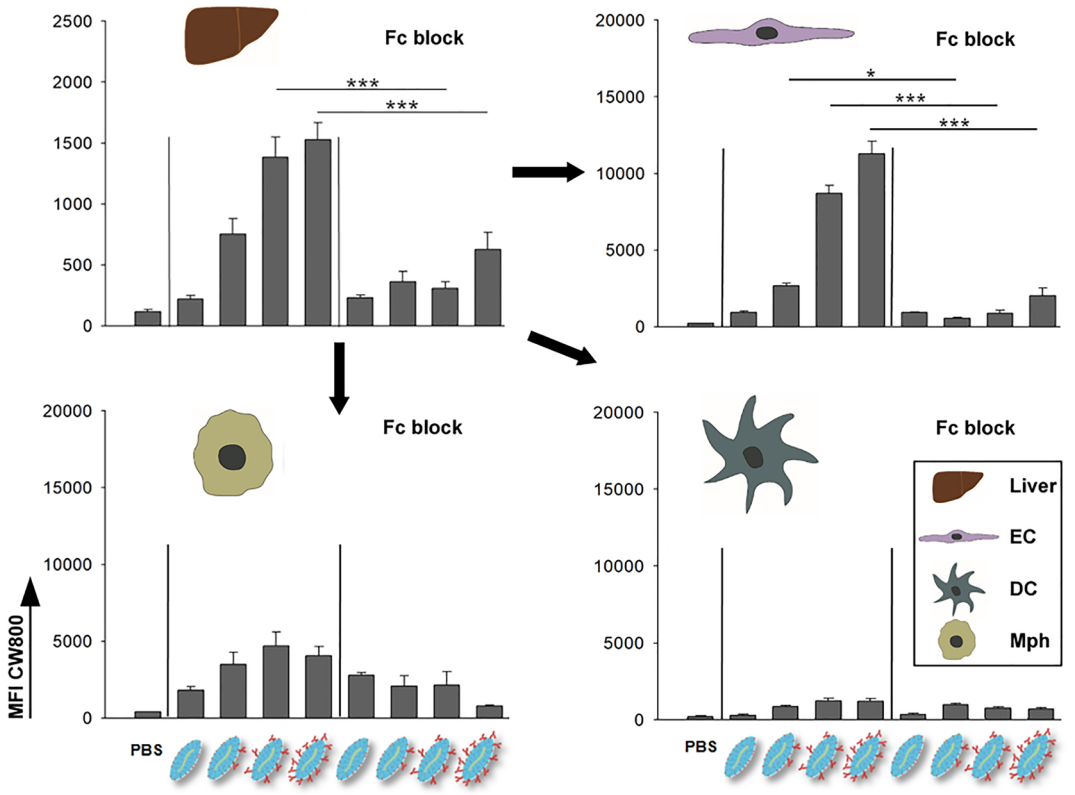

Figure 5. Systemic blockade of Fc receptors diminishes binding of PB−antibody conjugates to liver ECs. Mice were sequentially injected with Fc block and PB conjugates as described in the legend of Figure 4. Liver NPCs were prepared 24 hpi, and binding of CW800-labeled PB formulations (MFI) to either NPC population (liver endothelial cells (ECs: $CD45^{-}CD31^{+}$), macrophages (Mphs: $CD45^{+}F4/80^{+}$), and dendritic cells (DCs: $CD45^{+}CD11c^{+}$)) was assessed by flow cytometry (see legend of Figure 3A). Upper left panel: total liver NPCs, upper right panel: liver ECs, lower left panel: liver Mphs, lower right panel: liver DCs. Data denote the mean ± SEM (n = 6−8 obtained from 2 to 3 experiments; one-way ANOVA, $*p < 0.05$, $***p < 0.001$).

antibody numbers (Figure 4A). Again, each PB−antibody conjugate was associated with a higher fraction of liver ECs than Mphs. In contrast, liver DCs engaged with all PB−antibody conjugates at a comparable extent. Interestingly, *in vitro* blockade of Fc receptors using a commercially available CD16/CD32 (FcγRIIb/FcγRIII)-specific antibody,[37] for which the blocking efficiency was assessed beforehand (see Supp Figure 2), almost completely abrogated the binding of subsequently applied PB−antibody conjugates to ECs and Mphs, whereas their binding to DCs remained unaltered, suggesting that liver DCs mostly bound the NPs *via* specific interactions of the aDEC205 antibodies with their target, DEC205, whereas liver ECs and Mphs bound PBs *via* surface Fcγ receptors. This observation also indicates that within the liver EC population LSECs are largely responsible for binding of PB−antibody conjugates, since they are the only liver EC population that expresses FcγRIIb/FcγRIII.

To confirm the role of FcR-mediated accumulation of antibody-decorated PBs in the liver, we blocked FcR interactions by injection of 50 μg of CD16/CD32 (FcγRIIb/FcγRIII)-blocking antibodies, based on the results of a pre-experiment (see Supp Figure 3), prior to systemic application of PB conjugates *in vivo*. While FcR blockade had no effect on the amount of circulating PBs without antibody and in PB−aDEC205(2), significantly more PB−aDEC205(6) (2-fold) and PB−aDEC205(12) conjugates circulated in the blood at 6 hpi (up to 2.5-fold, Figure 4B). In agreement, FcR blockade had no effect on liver deposition of the PB conjugates with no and low antibody content, but drastically reduced liver accumulation of PB−antibody conjugates with intermediate and high antibody contents at 3 (Figure 4C, left panel) and 24 hpi (Figure 4C, right panel, D), resulting in a more uniform distribution of PB−aDEC205(6) and PB−aDEC205(12) within the animal (Figure 4C). We also calculated the relative fluorescence recovered from each organ. Here, it became apparent that PB accumulation in lymphatic organs (spleen, LN) inversely correlated with the number of attached antibodies. In contrast to the *in vitro* situation (Figure 4A), *in vivo* administration of Fc-blocking antibodies only partially reduced the dominant PB accumulation in the liver, but still improved accumulation of PBs in the spleen and LNs significantly, again—in line with our expectations—inversely correlating with the number of attached antibodies per PB [PB−aDEC205(2) > PB−aDEC205(6) > PB−aDEC205(12)].

Flow cytometric *ex vivo* analysis confirmed the almost abrogated binding of PB with intermediate or high antibody numbers to liver NPCs after FcR blockade (Figure 5, left upper panel, Supp Figure 4, left upper panel, Supp Figure 5A). Fc blockade strongly reduced binding of all PB−antibody conjugates to ECs at all time points investigated (Figure 5 and Supp Figure 4, Supp Figure 5B), whereas binding of PB−antibody conjugates to Mphs was significantly reduced only at 3 hpi (Supp Figure 4), but not at 24 hpi (Figure 5, Supp Figure 6), and binding of PBs to liver DCs was largely unaffected by Fc receptor blockade (Figure 5, Supp Figure 4, Supp Figure 6).

https://doi.org/10.1021/acsnano.1c05713
ACS Nano 2021, 15, 15191−15209

Taken together, these *in vivo* results confirm that LSECs are responsible for the retention of antibody-coated NPs in the liver *via* FcR-mediated binding of the antibodies' Fc part.

PB−Antibody Conjugates with Low, but Not with Intermediate or High Numbers of DC-Targeting Antibodies Are Enriched in Secondary Lymphoid Organs. An important prerequisite of NP-based immunotherapeutic approaches that target antigen-presenting cells is that the NPs reach secondary lymphoid organs, especially LNs and the spleen.[6] Therefore, we next assessed to what extent intravenously injected PBs that were functionalized with different amounts of aDEC205 antibodies were detectable in the spleen and LNs on a single-cell level in a time-dependent manner.

As also shown before (see Figure 2C), more PB−antibody conjugates were trapped in the liver when functionalized with 6 or 12 antibodies per NP (PB−aDEC205[6], PB−aDEC205[12]) than with 2 antibodies per NP (PB−aDEC205[2]) (Figure 6, left panel). In general, the frequencies of PB-positive NPCs were lower at 24 hpi *versus* 3 hpi, suggesting that antibody-coated NPs are only temporarily retained in the liver. In the spleen, 0.1−0.5% of *ex vivo* isolated whole spleen cells were PB-positive for either PB−antibody conjugate applied. Similar to liver NPCs, the frequency of PB-positive spleen cells decreased over time. Only few LN cells (<0.4%) engaged either PB−antibody conjugate when assessed at 3 hpi, whereas a significant percentage of LN cells (4%) had acquired PBs at 24 hpi when these had been functionalized with low amounts of antibodies (PB−aDEC205(2)). Importantly, LN accumulation of PBs decreased dramatically with increasing amounts of antibody per PB (Figure 6, right panel). Taken together, these observations suggest that in liver and spleen a fraction of PB−antibody conjugates is engaged by cells in a transient manner and that only PBs coated with 2 antibodies per NP, but not those with 6 and 12 antibodies per NP, accumulate in their target cells later on.

PBs with a Higher Antibody Number Display a More Pronounced Protein Corona, and Its Constituents May Engage Various Cellular Receptors. Since PB−antibody conjugates may transiently interact with cells *via* additional mechanisms besides Fc/FcR, we questioned the potential role of the protein corona in this regard. So far, many types of NPs have been shown to be coated by a protein corona, which may affect their cellular binding.[10] Alberg and co-workers have recently reported that PB polymers that were similar to those used in this study showed a very low adsorption of plasma components (less than 1 protein per NP),[24] which is in accordance with their long blood circulation half-life. We asked whether antibody-conjugated PBs would cause the formation of a more pronounced protein corona or the binding of specific proteins such as complement factors, and thereby increase the probability of (transient) PB binding to cellular receptors, *e.g.*, FcγRIIb/FcγRIII, additionally affecting their overall biodistribution. To this end, naked PBs or PBs conjugated with a high number of aDEC205 antibodies were incubated with plasma, and protein−PB complexes were separated by asymmetrical flow field-flow fractionation (AF4) as recently described.[24] The PB−antibody conjugate displayed an unaltered AF4 retention time, indicating that the amount of adsorbed proteins is low and thus does not affect their size (Supp Figure 7A) nor cause any aggregation. This was additionally confirmed by DLS measurements (Supp Figure 7B) in blood plasma. The highly sensitive silver staining of the SDS-PAGE electrophoresis identified, however, some binding

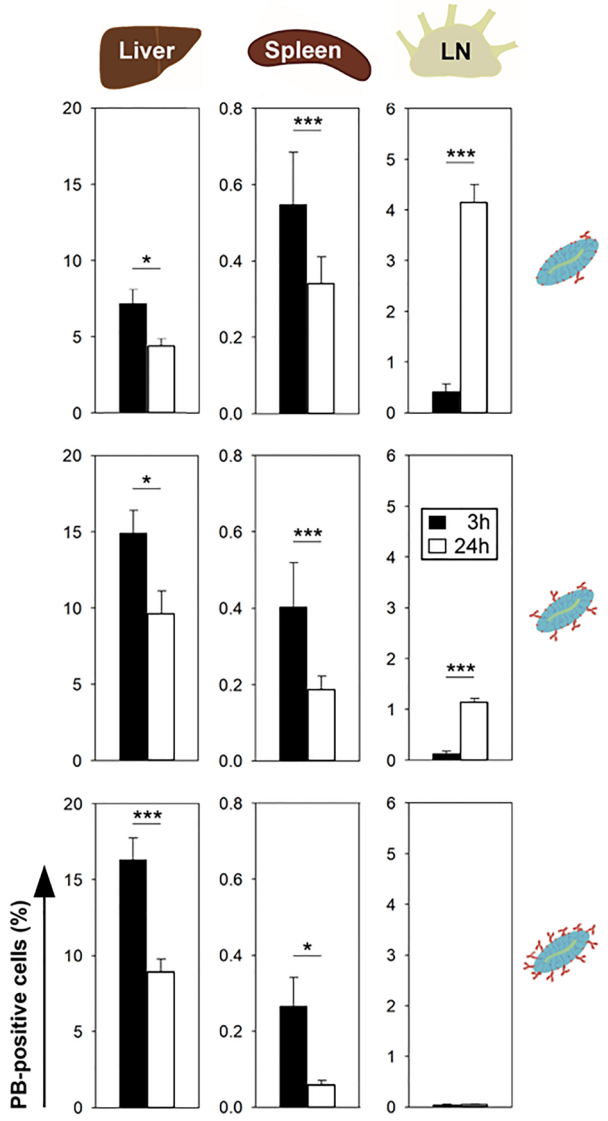

Figure 6. Liver accumulation of PB−antibody conjugates after systemic application decreases over time, paralleled by increased levels in lymph nodes in the case of low/intermediate PB antibody density. Mice were intravenously injected with PB formulations as described in the legend of Figure 2. After 3 hpi (black bars) and 24 hpi (white bars), liver, spleen, and LNs were retrieved. The frequencies of PB-positive cells of a given cell type within the relevant cell suspensions (liver NPC, total spleen, and LN cells) were assessed by flow cytometry. Data denote the mean ± SEM (n = 6−8, obtained from 2 to 3 experiments; one-way ANOVA, *p < 0.05, ***p < 0.001).

of proteins (60−80 kDa, 160−260 kDa) to the PB−aDEC205 conjugates (Supp Figure 7C).

Using mass spectroscopy, we were able to identify a total of 30 different proteins on naked PBs and 50 different proteins on aDEC205-conjugated PBs, although total amounts were very small in all cases. Among these, only seven proteins were identical (Figure 7A,B). Compared to naked PBs, significantly more protein bound to the surface of anti-DEC205-coated PBs (Figure 7B,C). In the protein corona of aDEC205-coated PBs, several genuine factors of the (classical) complement pathway and a number of immunoglobulins (Igs) were specifically enriched (Figure 7C, Supplemental Table 1). In this regard it is interesting to note that the constant regions of several Igs are

https://doi.org/10.1021/acsnano.1c05713
ACS Nano 2021, 15, 15191−15209

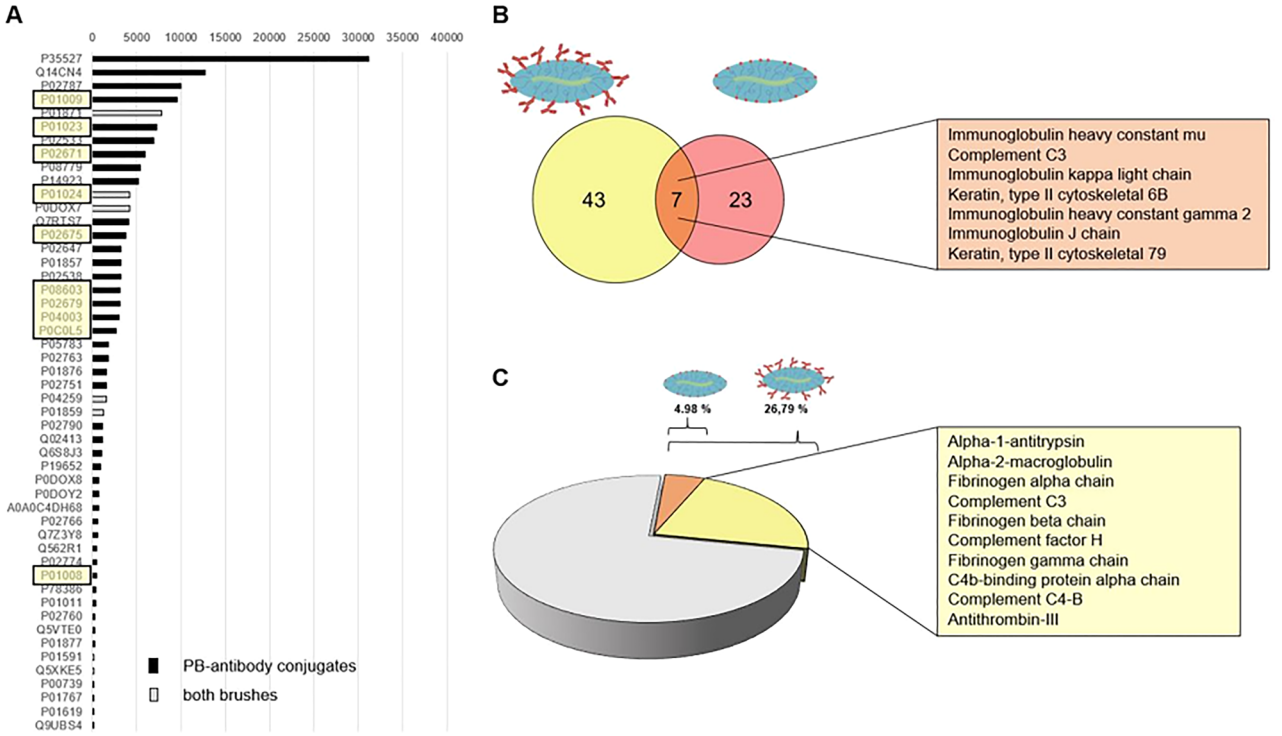

Figure 7. Antibody-induced protein corona formation: (A) Significantly enriched proteins associated with PB−antibody conjugate; (B) Venn diagram for enriched proteins in both controls on NPs. The overlap area shows the number of proteins significantly enriched on both NPs and (C) significantly enriched proteins related to the complement pathway and coagulation system in percentage of all identified proteins associated with the nanoparticle.

known to trigger the classical complement pathway.[38] Moreover, the protein corona of antibody-conjugated PBs also contained several factors that belong to the coagulation system, and four of these were shown to inhibit activation of the classical complement pathway.[39] We conclude that functionalization of PBs with high numbers of antibodies results in the formation of a distinct protein corona, which may contribute to the observed off-target accumulation and does not depend on specific Fc or Fab recognition. Since several corona proteins are known to engage with cellular receptors such as complement, immunoglobulin, and scavenger receptors, this provides an initial molecular explanation for further interactions of antibody-coated NPs with nontarget cells, including Fc receptors, complement, and coagulation factors, *in vitro* and *in vivo*.

The Effectiveness of DC Targeting Inversely Correlates with Antibody Number on the PB. We showed that in the liver the extent of accumulation of PBs correlated directly with the number of attached antibodies (see Figures 3, 4, and 5). In a complementary manner, the frequencies of PB-positive spleen (Figure 8) and LN cells (Supp Figure 8, upper panel) and even more obviously their overall MFI (LNs: Supp Figure 8, lower panel, spleen cells: Supp Figure 9) inversely correlated with the average antibody number per PB as assessed at 24 hpi. FcR blockade exerted no significant increase in frequencies of PB-positive cells or their MFI in either organ, indicating that PBs primarily bound to cells in lymphatic organs *via* specific interactions of the aDEC205 antibody with its cellular target DEC205. *In vitro* studies using bone-marrow-derived DCs confirmed that PB antibody conjugates engaged DCs to a comparable extent irrespective of their antibody density (Supp Figure 10). Blockade of Fc receptors had no major effect on binding of either PB formulation to DCs.

In the spleen, DEC205$^+$ DCs coexpress CD8a.[25] Thus, within the total DC population, CD8a$^+$ but not CD8a$^-$ DCs were specifically addressed by aDEC205-coated PBs (Figure 8). Notably, in both the spleen and LNs the extent of DC binding inversely correlated with the number of attached antibodies, presumably due to quantitative accumulation of PBs with intermediate/high antibody numbers as a first pass effect in the liver. Notably, more than 8% of the CD8a$^+$ DCs, compared to less than 1% of CD8a$^-$ DCs, in the spleen took up detectable numbers of PBs coated with an average of two aDEC205 antibodies, thus proving the high efficacy and selectivity of the DC targeting with antibody decorated NPs presented in this work.

In order to estimate the maximal number of antibody-conjugated PBs that engaged a DC, bone-marrow-derived DCs were incubated *in vitro* overnight with a high number of PB−aDEC205 antibodies labeled with AF647 or were left untreated. As assessed by flow cytometric analysis the whole cell population displayed a shift toward increased AF647 intensities (not shown), which indicated that all cells engaged PB antibody conjugates to varying extents. Concomitant analysis of serially diluted cell lysates and of PB−aDEC205(12) particles suggested that, on average, each DC had engaged about 50 000 PB−antibody conjugates when incubated with saturating NP doses (Supp Figure 11).

PB Conjugated with F(ab′)$_2$ Antibody Fragments No Longer Accumulate in the Liver, but Are Not Further Enriched in Secondary Lymphoid Organs. In order to corroborate our findings on the role of the Fc part of the attached antibodies for unwanted liver accumulation, we

https://doi.org/10.1021/acsnano.1c05713
ACS Nano 2021, 15, 15191−15209

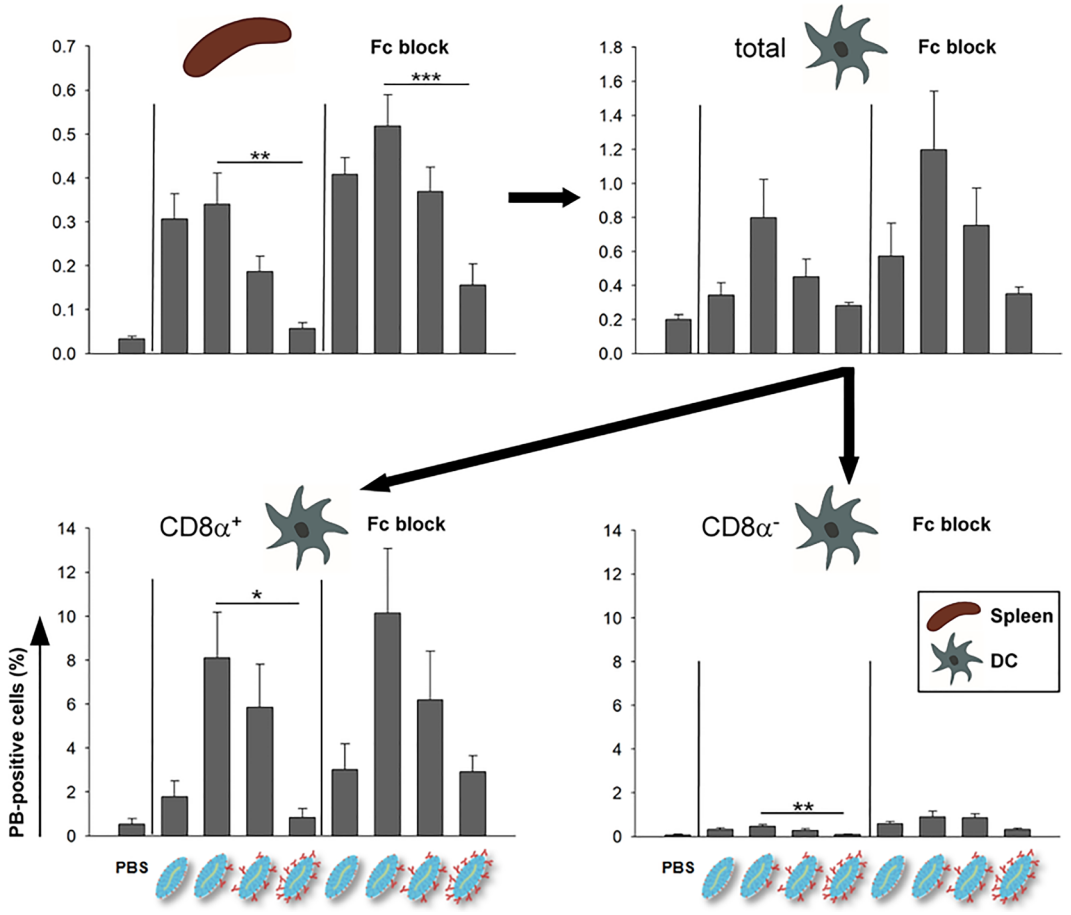

Figure 8. Systemically applied PB−antibody conjugates address splenic DCs most efficiently when equipped with low antibody numbers. Mice were treated with Fc block before i.v. injection of PB nanoparticles as described in the legend of Figure 4. Spleens were retrieved at 24 hpi, and frequencies of PB-positive spleen cells, total DCs ($CD11c^+$), and the $CD8a^+$ *versus* $CD8a^-$ DC populations within the splenic leukocyte population were delineated by flow cytometry. (A, B) Data denote the mean ± SEM (n = 6−8, obtained from 2 to 3 experiments; one-way ANOVA, *p < 0.05, **p < 0.01, ***p < 0.001).

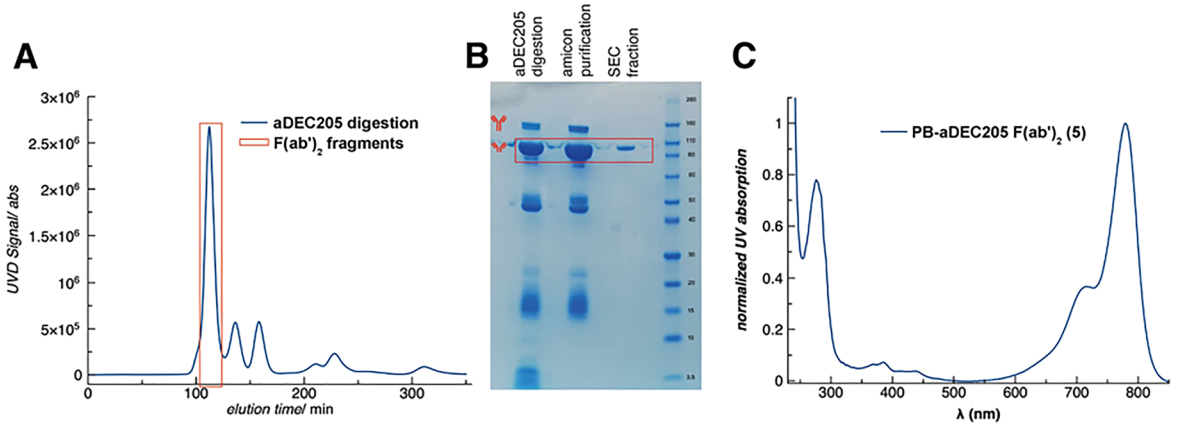

Figure 9. Synthesis and characterization of PB−$F(ab')_2$ antibody conjugates: (A) SEC elugram of aDEC205 digestion; (B) SDS PAGE of digestion and purified aDEC205 $F(ab')_2$ fragments of (1) digestion solution aDEC205, (2) digestion solution purified with Amicon spin filtration, (3) isolated $F(ab')_2$ fragments *via* SEC; (C) UV−vis analysis of the effectivity of PB−antibody conjugation.

conducted further biodistribution studies. We analyzed the biodistribution of PBs functionalized with an isotype control antibody bearing the same Fc part as the aDEC205 antibody, but lacking its specificity, and PBs conjugated with aDEC205 antibody lacking the Fc part (aDEC205-$F(ab')_2$), generated by enzymatic cleavage. We generated PBs with an intermediate number of antibodies per PB, which had resulted in pronounced Fc-mediated liver accumulation.

The aDEC205 antibody derived $F(ab')_2$ fragments were generated based on established protocols[40] (Supp Figure 12). aDEC205-derived $(Fab')_2$ fragments generated under optimized conditions were characterized by SEC elugrams (Figure 9A) and with SDS-PAGE (Figure 9B). The DBCO

https://doi.org/10.1021/acsnano.1c05713
ACS Nano 2021, 15, 15191−15209

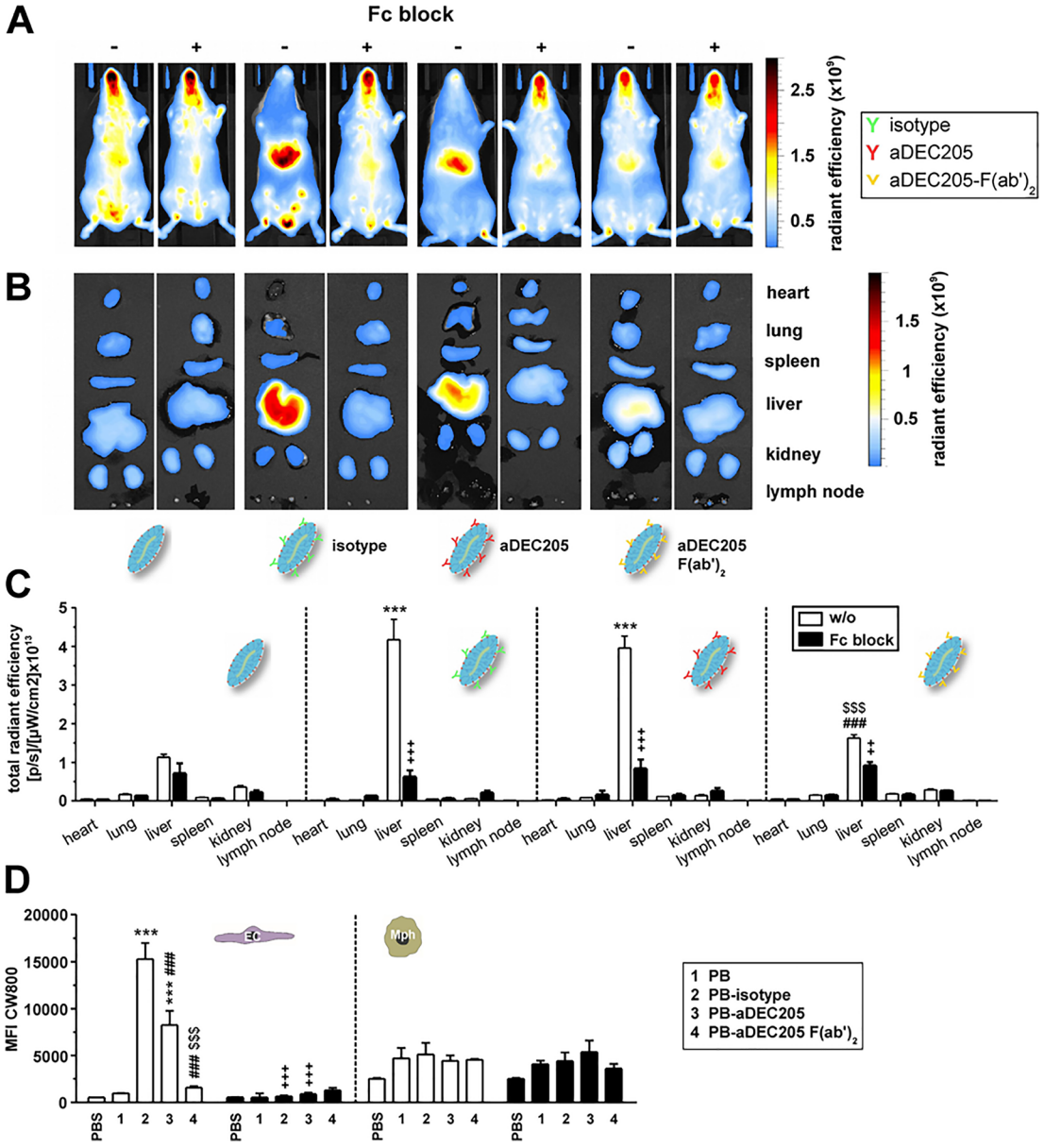

Figure 10. PBs conjugated with aDEC205 F(ab′)$_2$ antibody fragments do not accumulate in the liver. Mice were treated in parallel with PBs conjugated with full-length anti-DEC205 antibodies and derived F(ab′)$_2$ antibody fragments. PBs conjugated with a related full-length isotype control antibody and nonconjugated PBs served as controls. In parallel assays, mice were treated with Fc receptor blocking antibodies prior to administration of PB formulations. Distribution of PB formulations was assessed 3 hpi. (A) Fluorescence imaging of mice and (B) of retrieved organs. (A, B) Graphs are representative of 3 mice/group. (C) Quantification of organ-specific CW800 fluorescence (see B). (D) Binding of CW800-labeled PB formulations (MFI) to either liver NPC population (liver endothelial cells (ECs: CD45$^-$CD31$^+$) and macrophages (Mphs: CD45$^+$F4/80$^+$)) was assessed by flow cytometry (see legend of Figure 3A). (C, D) Data denote the mean ± SEM (n = 3; one-way ANOVA; **versus* nonconjugated PB, $^+$*versus* w/o Fc block of related formulation, $^\#$*versus* isotype control antibody-conjugated PB, $^\$$*versus* aDEC205-conjugated PB ($^+p < 0.05$, $^{***,+++,\#\#\#,\$\$\$}p < 0.001$).

modification and conjugation was performed as described before. An average number of five aDEC205 F(ab′)$_2$ fragments per PB was conjugated as confirmed by UV−vis spectroscopy (Figure 9C).

Since already with six antibodies binding to DCs reached its maximum in terms of % positive cells and MFI, we decided to compare PBs conjugated with the aDEC205 antibody, the related isotype control antibody (6 antibodies each per PB), and an aDEC205-derived F(ab′)$_2$ fragment (5 antibodies per PB) and nonconjugated PBs and applied them systemically to mice. In parallel settings, mice were pretreated with FcR-blocking antibodies. PBs conjugated with either the isotype control antibody or the full-length aDEC205 antibody predominantly accumulated in the liver as assessed 3 hpi (Figure 10A−C). In contrast, PBs conjugated with aDEC205-F(ab′)$_2$ showed significantly lower enrichment in the liver than PBs conjugated with full-length antibodies (isotype or aDEC205) and were comparable to nonfunctionalized PBs. As expected, pretreatment of mice with Fc receptor blocking antibodies resulted in strongly attenuated liver accumulation of the two PBs conjugated with either full-length antibody but only slightly reduced liver accumulation of PBs conjugated with aDEC205-F(ab′)$_2$. In the liver, PBs functionalized with either full-length antibody (isotype, aDEC205) predominantly

https://doi.org/10.1021/acsnano.1c05713
ACS Nano 2021, 15, 15191−15209

engaged ECs (Figure 10D), whereas PBs conjugated with aDEC205-F(ab′)$_2$ displayed no major binding. Liver Mphs engaged all PBs to some extent, irrespective of a conjugated antibody. Blockade of FcR prior to injection of PB formulations strongly reduced binding of each full antibody−PB conjugate to liver ECs, whereas no effect was observed for liver Mphs.

These results confirm that at a higher antibody number per PB the antibodies' Fc part strongly contributes to liver accumulation of systemically applied PBs, predominantly mediated by liver endothelial cells. However, also PBs conjugated with aDEC205-F(ab′)$_2$ displayed some liver accumulation in F4/80$^+$ liver Mphs (Figure 10, Supp Figure 13), which may be attributed to Kupffer cells,[33] which constitute the vast majority of liver Mphs.[34] Despite lower liver accumulation of PB−aDEC205-F(ab′)$_2$ as compared to PBs conjugated with aDEC205 full antibody (see Figure 10 A−C), we observed only a slightly enhanced targeting efficacy to DCs in the spleen or LNs. In line with this finding, the overall frequencies of PB-positive CD8a$^+$ DCs (Supp Figure 13C) were not higher than the ones achieved using PBs conjugated with a low number (2) of aDEC205 antibodies (see Figure 8), which may be attributed to a reduced stability of F(ab′)$_2$ fragments compared to full antibodies.

In summary, PBs with a low antibody number are superior to those with intermediate/high numbers of antibody or intermediate numbers of F(ab′)$_2$ fragments for targeting of DCs in secondary lymphoid organs, since antibody-coated PBs with >2 antibodies per PB are trapped by LSECs in the liver in a FcR-mediated fashion, depleting PBs from circulation and thus preventing them from reaching their target cells. Interestingly, PBs with an average of 2 aDEC205 antibodies per NP effectively target DCs in secondary lymphoid organs, reaching a total of 10% positive CD8α^+ DCs in the spleen and around 5% in LNs.

Liver entrapment is a common outcome of systemic NP application,[32] both for nonfunctionalized NPs[41] and for NPs that are surface-functionalized with antibodies.[42] Our study aimed to delineate the number of antibodies per NP as a determinant for undesirable liver accumulation *versus* the desired antibody-mediated target cell specificity in secondary lymphoid organs. For this, we employed PBs that are characterized by minimal cellular interactions and subsequently long plasma circulation half-life and allow fine-tunable attachment of antibodies at lysine residues in an adjustable and well-reproducible manner. We chose a very common method of antibody attachment that utilizes the strain-promoted azide−alkyne coupling reactions between a DBCO-modified antibody and azide-containing polypept(o)-ide-based molecular polymer brushes based on a polylysine backbone (DP = 250) and polysarcosine side chains (DP = 100). The binding affinity of the modified DEC205 antibody was not affected by this ligation type,[43] and the Fc domain remains—most likely—accessible. The robust synthetic approach chosen in this study[41−43] enabled us to adjust the average antibody number per particle, an important prerequisite for comparative analysis. The polymer brushes used for the synthesis of different PB−antibody conjugates as well as the number of near-infrared (NIR) dyes used for *in vivo* and *ex vivo* tracking were identical for all the different systems, enabling an unbiased comparative analysis. The various PBs were conjugated with the NIR dye CW800 since such dyes were shown to confer deep tissue penetration at low background.[44] This enables *in vivo* tracking of NPs and thereby also *ex vivo* quantification of NP accumulation in tissues. In addition, NIR dyes, including the CW800, are also detectable by flow cytometry,[45] which allows assessment of cell type-specific NP binding and uptake.[46]

We show that PBs conjugated with an average of only two antibodies on one hand displayed only moderate liver accumulation and, on the other hand, efficiently addressed DCs in secondary lymphatic organs. In contrast, PBs conjugated with higher numbers of antibody (6, 12) predominantly accumulated in the liver. We demonstrate that liver ECs contribute at much higher extent to liver entrapment of antibody-coated PB nanoparticles than F4/80$^+$ liver Mphs. We also demonstrate that LSECs—and to a much lesser extent also liver Mphs —bind the Fc part of PB-conjugated aDEC205 antibodies *via* FcR expressed on the surface of these cells. FcR blockade *in vitro* on isolated liver NPCs almost completely abolished binding of PB−antibody conjugates to LSECs and Mphs. Likewise, FcR blockade *in vivo* also potently reduced liver entrapment of subsequently applied PB−antibody conjugates.

So far, in most studies the liver-resident Mph population (mainly Kupffer cells) has been described as the main NP binding cell population in the liver.[47] In contrast, the contribution of LSECs in this regard is just becoming elucidated.[48] This cell population internalizes PB−antibody conjugates most likely *via* FcγRIIB since LSECs express only this FcR and since LSECs were reported to facilitate uptake of IgG immune complexes *via* FcγRIIB.[35] Similar to Mphs, LSECs are also equipped with various pattern recognition receptors, *e.g.*, of the C-type lectin family such as the mannose receptor[49] and L-SIGN[50] as well as different scavenger receptors.[51,52] Consequently, ECs compete with Mphs for NP uptake, as also indicated by zebrafish embryo studies published by Hayashi and co-workers.[53] These sets of surface receptors enable efficient binding and uptake of a vast array of exogenous material *via* endocytosis, including viruses such as HIV-1[54] whose size is on the same order of magnitude as that of PB-antibody conjugates (see Figure 1E). Therefore, LSECs may considerably contribute to the frequently observed liver entrapment of different types of NPs coated with antibodies[55] or carbohydrates,[56] since besides FcR-mediated mechanisms, liver accumulation can also result from recognition of NP surface structures by pattern recognition receptors such as mannose[57] and scavenger receptors.[53,58] Thus, surface functionalization of nanovaccines should account for immunoglobulin, carbohydrate, and scavenger receptors expressed at high density by LSECs and liver Mphs.[57,58] The adequate form of stealth providing polymers can further contribute to a long blood circulation by preventing NP uptake by liver ECs or other immune cells.[59] Notably, Sivaram and colleagues demonstrated in studies on the organ and cell level that there might be a "sweet spot" for the optimal balance between targeting and stealth effects.[60] Furthermore, it is well established that cellular interactions and *in vivo* biodistribution of NPs may be affected by a protein corona consisting of adsorbed serum constituents,[10] as exemplified here for PBs with a high density of full-length antibody (see Figure 7).

The protein corona of antibody-functionalized PBs is composed of Igs, components of the (classical) complement pathway, and the coagulation system (Supplementary Table 1), known to interact with the complement pathway.[39] In contrast, nonfunctionalized PBs bound very few serum proteins on their

https://doi.org/10.1021/acsnano.1c05713
ACS Nano 2021, 15, 15191−15209

surface, which may well be one reason for the long plasma half-life of naked PBs (Figure 2). The composition of the protein corona of antibody-conjugated PBs suggests that these NPs are recognized by natural antibodies,[61] which may trigger activation of the classical complement pathway,[62] negatively controlled by several factors of the coagulation system.[39] These findings suggest that the protein corona formed around PBs with high antibody density may further aggravate binding to FcR-expressing cells within the liver *via* the exposed Fc part of conjugated aDEC205 antibodies and adsorbed natural antibodies. In addition, these and other corona proteins on antibody-coated NPs may bind to additional cell surface receptors expressed by other cell types throughout the body, which may be one reason that we observed no increase in target cell binding of PBs after FcR blockade *in vivo* (Figure 8).

We also observed that numbers of PB−antibody conjugates that were trapped in the liver or spleen decreased over time (Figure 6), whereas a time-dependent decrease in PB−antibody conjugate deposition was not observed for isolated splenic DCs (data not shown). In parallel, PB−antibody conjugates with low, but not with high antibody density accumulated in LNs over time. We speculate that this may be due to redistribution of PB particles from the liver to the LNs, where $CD205^+$ cDC1 target cells are relatively abundant, or because of much slower transport of macromolecules within the lymphatic system compared to blood.[63] In contrast, PB−aDEC205(12) disappeared from the liver and spleen over time without accumulating in LNs, which suggests that high-avidity PB−aDEC205(12) antibody conjugates may subsequently bind other cell types throughout the body, potentially *via* protein corona induced interactions as outlined above, thus preventing their time-dependent redistribution toward their target cells.

In order to avoid FcR binding and liver accumulation, natural or engineered antibody fragments devoid of the Fc region, such as Fab fragments and single-chain Fv fragments[64] as well as other epitope-binding moieties such as affibodies[65] or aptamers,[66] may provide another pathway to circumvent liver accumulation of targeted NPs.[64] In accordance, we show that PBs conjugated with five $F(ab')_2$ fragments of aDEC205 displayed much lower liver accumulation as compared to PBs conjugated with the same number of isotype control antibody and aDEC205 full-length antibody, respectively.

However, full antibodies do not need expensive engineering, and several of them are commercially available in GMP grade, thus facilitating clinical translation. Furthermore, the Fc part may play an additional functional role as exemplified for agonistic CD40 antibodies, which require the Fc part to trigger target cell stimulation.[67] FcR-mediated effects may be circumvented by using peptides that specifically bind to the Fc region of antibodies, as demonstrated by Kedmi and coworkers for the modification of liposomes.[68] Moreover, Mailänder and co-workers have recently shown that polystyrene NPs preadsorbed with an anti-CD63 antibody retained receptor-specific targeting *ex vivo*.[69] Most importantly, since we demonstrate here that an average of two antibodies per NP is both sufficient for target cell engagement and necessary to avoid nonspecific accumulation in other organs such as the liver, careful control of the number of antibodies per NP may be generally advisable to enhance target cell specificity of antibody-coated NPs.

As mentioned above we are not aware of other comparative studies that identified the number or density of full-length antibodies on long circulating synthetic NPs as a determinant of unspecific liver accumulation *versus* cell type-specific targeting. However, effects of the number/density of receptor-targeting peptides per NP on their biodistribution have been addressed in several studies. For example, NP derivatives decorated with a prostate-specific membrane antigen binding aptamer for tumor cell targeting accumulated preferably in the liver in correlation with aptamer density, but not in the spleen. The underlying mechanism, however, was not assessed. In another study, liposomal formulations decorated with various densities of CD38 and CD138 receptor binding peptides, respectively, for engagement of myeloma cells showed a density-dependent increase (CD38) or decrease (CD138) in tumor cell binding as compared to nontargeting liposomes.[70] Accumulation of these formulations in other organs, including the liver, was not affected by the density of either peptide. Similarly, for nanohydrogels, which accumulated predominantly in the liver and spleen, conjugation with "high" amounts of epidermal growth factor receptor-binding peptides elevated tumor targeting, but had no effect on their predominant accumulation in the liver and spleen.[71] Concerning the targeting behavior of NPs decorated with various numbers of full-length antibodies, Zern and co-workers reported that a moderate number of ICAM-1-specific antibodies per NP achieved a better targeting specificity of inflamed vasculature expressing ICAM-1 than NPs decorated with high antibody numbers.[14,17] In aggregate, these studies underscore that NPs conjugated with receptor-binding peptides may accumulate in the liver as well and that the density of targeting units plays a role in this regard. So far, several strategies, including PEGylation and decoration with proteins such as CD47 serving as a "don't-eat-me" signal, have been developed to minimize unspecific NP uptake by liver NPCs.[10] For example, Samuelsson and co-workers demonstrated that PEGylation of liposomes strongly reduced their uptake by Kupffer cells in the liver as well as spleen accumulation and thereby significantly elevated their concentration in the blood.[47] Similarly, Zhou and coworkers reported that PEGylated PLGA-based NPs equipped with a second PEG layer minimized binding to Kupffer cells as well as LSECs.[59] It remains, however, an open question whether this approach can be combined with active targeting and improve NP accumulation at their target cells. In addition, the combination of various ligands may induce secondary effects, *e.g.*, protein corona formation. As an alternative strategy, we could show that modification of the size and zeta potential of mRNA-containing lipoplexes determined their accumulation in the liver or spleen as well as efficient targeting and transfection of splenic DCs without the necessity of a DC-targeting structure on the NP surface.[72]

CONCLUSIONS

The aim of this study was to investigate to what extent the decoration of NPs with targeting antibodies can induce off-target accumulation, *e.g.*, in the liver, upon intravenous application of NPs. To demonstrate this, we generated polysarcosine-based polymer brushes with distinct average antibody numbers ranging from a "low" (2 molecules), to "intermediate" (6 molecules) and a "high" amount (12 molecules). These conjugates were similar in size and free of unbound antibodies. We were able to show that an average of two antibodies per NP are sufficient to reach an acceptable percentage of target cells in lymphoid organs while bypassing

https://doi.org/10.1021/acsnano.1c05713
ACS Nano 2021, 15, 15191−15209

the liver. PBs decorated with more than two antibodies accumulate rapidly in the liver due to recognition by FcRs or complement receptors as demonstrated by *in vivo* studies and *ex vivo* analysis of the nanoparticle-associated protein corona. We demonstrate that liver accumulation of antibody-coated NPs is mostly due to binding of PB conjugates to FcRs expressed on LSECs. Most importantly, capture of antibody-coated NPs by LSECs can be greatly reduced if antibody numbers per NP are kept low or if $F(ab')_2$ antibody fragments are used, thus preventing liver accumulation while retaining effective target-specific binding to DEC205 on DCs in secondary lymphatic organs. Since LSECs are potent inducers of antigen-specific tolerance, nanovaccines intended to induce immunity should minimize uptake by LSECs and other FcR-expressing cells in order to prevent tolerance induction, which underlines the importance of controlling antibody numbers on synthetic nanoparticle-based vaccines. Due to their enhanced circulation half-life, minimal entrapment in the liver, and effective binding to their target cells, PBs with an average of two full aDEC205 antibodies as well as $F(ab)_2$ fragments thereof seem to be a suitable platform for the development of DC-targeting nanovaccines for systemic applications.

MATERIALS AND METHODS

Peptobrush Synthesis. *Synthesis of Sarcosine N-Carboxyanhydride (NCA).* Synthesis of sarcosine NCA was performed as described with some modifications.[21,27,73] First, 20.52 g (230.2 mmol) of sarcosine (dried under vacuum for 1 h) was weighed into a three-neck, round-bottom flask. Then, 300 mL of absolute THF (tetrahydrofuran) was added under a nitrogen flow, and 184 mmol of diphosgene were added using a syringe. This solution was mildly refluxed for 3 h. The outlet was connected to two gas washing bottles containing an aqueous NaOH solution to neutralize phosgene, and dry nitrogen was led through the solution for 3 h. The obtained brownish oil was dried under reduced pressure (1×10^{-3} mbar for 2 h). The obtained amorphous solid crude product was redissolved in 40 mL of THF and was precipitated using 300 mL of dry hexane. The solution was stored overnight in a −20 °C freezer. On the next day, the precipitated product was filtered under a dry nitrogen atmosphere and dried sequentially for 60−90 min using dry nitrogen and for 2 h under high vacuum in a sublimation apparatus. Then, the product was sublimated (85 °C, 1×10^{-3} mbar) and was collected from the sublimation apparatus in a glovebox on the same day. The purified product (156 mmol, 68% yield, constituting colorless crystallites with a melting point of 102−104 °C (lit:[78] 102−105 °C)) was stored in a Schlenk tube at −80 °C and was handled in a glovebox at all times. ^{1}H NMR (300 MHz, $CDCl_3$): δ [ppm] = 4.22 (2 H, s, $-CH_2-CO-$), 2.86 (3 H, s, $-CH_3$).

Synthesis of Azidobutyric Acid Pentafluorphenylester. γ-Azidobutyric acid (7.74 mmol) was dissolved in predried THF, and triethylamine (15.0 mmol, 2 equiv) was added. The solution was stirred at room temperature (RT) for 30 min. Then, two volumes of pentafluorophenol trifluoroacetate (15.0 mmol) were added dropwise. The reaction mixture was stirred overnight at RT. Completion of the reaction was evaluated with TLC (thin-layer chromatography). THF was distilled, and the remaining solid was first dissolved in dichloromethane and then was extracted three times with water. The organic phase was dried with $MgSO_4$, and DCM (dichloromethane) was distilled off the product. The product was purified by column chromatography.

^{1}H NMR (400 MHz, $CDCl_3$): δ [ppm] = 3.46 (2 H, t, $-CH_2-CH_2-\mathbf{CH_2}-N_3$), 2.80 (2 H, t, $-\mathbf{CH_2}-CH_2-CH_2-N_3$), 2.05 (2 H, m, $-CH_2-\mathbf{CH_2}-CH_2-N_3$). ^{19}F NMR (400 MHz, $CDCl_3$): δ [ppm] = −153.95 (2F, d, *o*-CF), −158.90 (1F, t, *p*-CF), −163.32 (2F, t, *m*-CF).

PB Synthesis. The synthesis was performed as described with some modifications.[26] The following stock solutions were prepared directly prior to use under a dry nitrogen atmosphere: 228 mg mL^{-1} DIPEA (diisopropylethylamine) in 3.7 mL of DMF (dimethylformamide), 7.83 g sarcosine NCA in 40 mL of DMF, and 218 mg of azidobutyric acid pentafluorphenylester in 2 mL of DMF. The following operations were performed under a steady flow of dry nitrogen. A 0.80 mL (351 μmol) amount of DIPEA−DMF was added *via* syringe to a Schlenk tube containing 71 mg (292 μmol) of poly(L-lysine trifluoroacetate) (DP = 258) dissolved in 2 mL of DMF solution. After 1 h stirring, 16.8 mL (29 mmol) of sarcosine NCA in DMF was added. The solution was stirred at RT and kept at a constant pressure of 1.25 bar of dry nitrogen *via* a Schlenk line to prevent impurities from entering the reaction vessel while allowing CO_2 to escape. When the reaction was finished (completion of the reaction was confirmed by IR spectroscopy by the disappearance of the NCA peaks), 0.95 mL of azidobutyric acid pentafluorphenylester in DMF (1.2-fold excess based on the amine groups) was added, and the reaction mixture was stirred for 2 days at 40 °C. The final azide-functionalized polymer brush was precipitated in ether and centrifuged (4500 rpm at 4 °C for 15 min). After discarding the liquid fraction, fresh ether was added and the polymer was resuspended using a sonic bath. The suspension was centrifuged again, and the procedure was repeated. The polymer was dissolved in Milli-Q water and purified using Amicon Ultra centrifugal filters (50 kDa, 4000*g*, 4 × 20 min). After lyophilization, a colorless product was obtained. Yield: 63%.

Dye Labeling of PBs. The dyes AlexaFluor647-DBCO and 800CW-DBCO were conjugated to the PBs *via* SPAAC. In a typical experiment, the PB was dissolved in DPBS (Dulbecco's phosphate-buffered saline) (c_{PB} = 50 g·L^{-1}) and the dye was dissolved in DMSO (c_{Dye} = 5 mM). As the reaction is quantitative, 1 equiv of the desired amount of dyes per brush was added. After incubation overnight at RT under light exclusion, the reaction mixture was purified by Amicon Ultra centrifugal filter devices to remove unbound dye (15 mL, 50 kDa, 4000*g*, 10 times). The resulting solution was concentrated with Amicon Ultra centrifugal filter devices (50 kDa, 4000*g*) and filtered through sterile 0.22 μm Millex-GS filters. R_h was measured by DLS and FCS (fluorescence correlation spectroscopy). FCS was also used to prove the absence of unconjugated dye and to determine the number of dyes per brush. To evaluate quenching effects, emission spectra of the free dye and the dye-labeled PBs were recorded, using solutions of the same optical density. If quenching effects were detected, the number of dyes determined by FCS were corrected by the extent of quenching.

Synthesis of DBCO-Functionalized aDEC205. In a typical experiment, 2 equiv of DBCO-PEG_4-NHS-ester (dissolved in DMSO [dimethyl sulfoxide], c = 10 g·L^{-1}) was added to the antibodies. aDEC205 and ratIgG2a were used as received (dissolved in DPBS, $c_{aDEC205}$ = 4−7 g/L). After incubation overnight at RT, the reaction mixture was purified by Amicon Ultra centrifugal filter devices (15 mL, 10 kDa, 4000*g*, 10 times) to remove unbound DBCO-PEG_4-NHS-ester and NHS. Afterward, preparative size-exclusion chromatography was performed using a Sepharose 4 FF XK 16/70 column (flow 0.5 mL·min^{-1}) to remove aggregates (aDEC205-DBCO fraction, 80−110 mL). The resulting solution was concentrated with Amicon Ultra centrifugal filter devices (10 kDa, 4000*g*) and filtered through sterile 0.22 μm Millex-GS filters. $R_{h,antibody\text{-}DBCO}$ = 5−6 nm. The antibody concentrations as well as the number of DBCO per bioactive component were determined by UV−vis spectroscopy as described in the literature.

Synthesis of Dye-Labeled PLys250. PLys258 (20 mg, 320 nmol) was dissolved in 2 mL of DPBS, and AlexaFluor647-NHS ester (2.5 equiv, 1 mg, 800 nmol) dissolved in DMSO (160 μL) was added. The reaction mixture was incubated overnight under light exclusion at RT. The reaction product was purified using Amicon Ultra centrifugal filter devices (15 mL, 10 kDa, 4000*g*, 20 times). R_h(FCS) = 7.6 nm. Each molecule contained two dye residues as determined by FCS. FCS analysis demonstrated that the solution contained 15% free dye, taken into account for calculations of the dye concentrations. The pLys concentration was determined by dividing the dye concentration of the conjugated dye by 2.

https://doi.org/10.1021/acsnano.1c05713
ACS Nano 2021, 15, 15191−15209

Synthesis of Dye-Labeled aDEC205. In a typical experiment, 2 equiv of AlexaFluor647-NHS ester (dissolved in DMSO, c = 5 mM) was added to the antibodies, respectively. aDEC205 antibody (clone NLDC145) was used as received (dissolved in DPBS, $c_{\alpha DEC205}$ = 4−7 g/L). After incubation overnight at RT, the reaction mixture was purified using Amicon Ultra centrifugal filter devices (15 mL, 10 kDa, 4000*g*, 10 times) to remove unbound AlexaFluor647-NHS ester and NHS. The resulting solution was filtered sequentially through Anotop 20 nm filters and sterile 0.22 μm Millex-GS filters. $R_{h,antibody\text{-}FD}$ = 5−6 nm. FCS shows that there is still 15−20% free dye in the solution. The antibody concentration is calculated from the UV−vis spectrum using the specific antibody absorption at 280 nm.

Synthesis of PB Conjugates with aDEC205, ratIgG2a, and aDEC205 F(ab')$_2$ Fragments. aDEC205-derived F(ab')$_2$ fragments were generated according to established protocols with modifications.[74] A 36.3 mg amount of aDEC205 (0.24 μM) was transferred into 0.2 M sodium acetate buffer using Amicon Ultra centrifugal filter devices (15 mL, 10 kDa, 4000*g*, 5 times). Pepsin was dissolved in the same buffer, getting a concentration of 10 mg/mL. After several small-scale pilot digestions with final w/w ratios of pepsin to antibody from 1:1 to 1:1000, the large-scale digestion was performed with a final w/w ratio of pepsin to antibody of 1:4 at 37 °C and 550 rpm. After incubation the pH was adjusted to 7.8 with 2 M Trizma base to stop the reaction. Digestion progress was determined *via* SDS-PAGE (sodium dodecyl sulfate polyacrylamide gel electrophoresis). To isolate the F(ab)$_2$ fragments a size-exclusion chromatography was performed using a HiPrep 16/60 Sephacryl S-500 HR column (sterile DPBS, flow 0.5 mL·min^{-1}). The fractions 105−125 min were concentrated with Amicon Ultra centrifugal filter devices (15 mL, 10 kDa, 4000*g*) and filtered through sterile 0.22 μm Millex-GV filters. The purified F(ab)$_2$ fragment was DBCO modified as described before.

Antibody conjugates comprising 2, 6, 10, and 12 aDEC205 antibodies per PB and an intermediate number of rat IgG2a and F(ab)$_2$ fragments, respectively, were synthesized. The amount of the DBCO-modified antibody that was added to the brush depends on the number of DBCO (N_{DBCO}) per component; $1/(0.34N_{DBCO})$ equiv of the DBCO-modified component (dissolved in DPBS, $c_{antibody\text{-}DBCO}$ = 5−15 g·L^{-1}) was added to the dye-labeled brush dissolved in DPBS (c_{PB} = 1 × 10^{-5} to 1 × 10^{-6} M). The reaction mixture was incubated overnight at RT. To remove bridged brushes and unconjugated antibodies, PB conjugates were purified *via* preparative SEC using a Sepharose 4 FF XK 16/70 column (flow 0.5 mL·min^{-1}). The fraction from 55 to 75 mL was collected, concentrated using Amicon Ultra centrifugal filter devices (50 kDa, 4000*g*), and filtered through sterile 0.22 μm Millex-GS filters. Each conjugate was analyzed by DLS, FCS, UV−vis spectroscopy, and SDS-PAGE.

Biological Materials and Assays. *Animals.* Female C57/Bl6 (*in vitro* studies) and BALB/c (*in vivo* studies) mice were purchased from Envigo.

Antibodies. CD45-FITC (Invitrogen), CD31-PE (eBioscience), CD146-APC (Biolegend), CD11c-APC (eBioscience), F4/80-eFluor450 (Invitrogen), CD19-AF488 (eBioscience), CD8a-PE (BD Pharmingen), aCD16/CD32 (clone 2.4G2), and *in vivo* ready anti-mouse CD16/CD32 and isotype control (TONBO Bioscience) were obtained.

Isolation of Liver NPCs. Liver NPCs of female C57/Bl6 and BALB/c mice were isolated by an organ perfusion method including collagenase digestion as previously described.[70] In short, mice were anesthetized with a ketamine/rompun mixture, and the abdominal cavity was opened. By cannulating the *vena portae*, 20 mL of HBSS (Hank's balanced salt solution) (ThermoFisher Scientific) containing collagenase A (Sigma-Aldrich) and DNase I (Sigma-Aldrich) flushed the liver after the aorta had been cut. The liver, largely devoid of erythrocytes or other loosely bound cells, was then dissected into pieces and incubated for 15 min at 37 °C in a 50 mL tube containing the perfusion enzyme solution. After incubation the liver was put through a 70 μm nylon cell strainer and the enzymatic reaction was stopped with medium (DMEM (Dulbecco's modified Eagle medium)/F-12 GlutaMAX, ThermoFisher Scientific). To remove hepatocytes, the cell suspension was centrifuged at 300*g* for 15 min. The remaining cells in the suspension were further purified by 30% Histodenz−HBSS gradient centrifugation as specified before.[75] The obtained liver NPCs were then either cultured in medium (DMEM/F-12, GlutaMAX, ThermoFisher Scientific) (described in the following section) or subjected to antibody staining for subsequent flow cytometry analysis. For *ex vivo* studies the liver dissociation kit from Milteny was used following the instructions.

In Vitro NP Incubation. After isolation, NPCs were seeded into a nontreated 12-well plate in a volume of 1 mL and 1 million cells per well. NPCs were treated with different brush−antibody conjugates at 37 °C for 1 h. For this 10^{12} particles were used. Following incubation, NPCs were rinsed on ice and transferred to flow cytometry tubes for staining.

Flow Cytometry. Single-cell suspensions of respective organs were obtained after mechanical digestion and filtering using a 70 μm nylon cell strainer. Livers were digested previously using the liver dissociation kit (Milteny). After lysis of erythrocytes (liver, spleen), cells were incubated with receptor-specific antibodies for FACS analysis. For this, cells were washed (2% FCS in DPBS), and FcRs were blocked with aCD16/CD32 (2.4G2 clone) for 10 min. Afterward, liver NPCs were incubated with receptor-specific antibodies (CD45-FITC, CD31-PE, CD11c-APC, and F4/80-eFluor450) for 20 min at 4 °C. Within the CD45$^+$ liver NPC fraction, DCs (CD11c$^+$), ECs (CD31$^+$), and Mphs (F4/80$^+$) were identified according to the expression of their corresponding lineage marker. Spleen and LN cells were incubated with anti-CD11c-APC to detect DCs and in the case of spleen cells in addition with anti-CD8a-PE to differentiate CD8a$^+$ and CD8a$^-$ DC subpopulations. All antibodies were obtained from Thermo Scientific. Cells were fixed with 0.7% PFA and subjected to flow cytometry (Attune NxT flow cytometer, Thermo Scientific). Results were evaluated with Attune NxT flow cytometer software.

cLSM (Confocal Laser Scanning Microscopy). Liver NPCs were incubated with 10^{12} particles for 1 h at 37 °C as described above. After washing the cells with PBS, Hoechst dye (2 μM) was added and samples were incubated at RT for 30 min to stain the nucleus. To flag LSECs, samples were incubated with a CD146-specific antibody (APC-labeled) for 20 min at 4 °C. Cells were washed twice with DPBS, and images were taken using a TCS SP5 confocal microscope at the Institute of Molecular Biology, Mainz.

Biodistribution and Blood Circulation. The PB−antibody conjugates (0.5−1.8 mg, equimolar amounts of PBs) and FcR blocking antibody (anti-CD16/CD32;[37] 50 μg) were injected i.v. into BALB/c mice. Particle injection followed 3 h after injection of the blocking antibody. The animals were imaged at the indicated time points using the IVIS Spectrum Imaging System (PerkinElmer) with the excitation/emission filter set of 745/800 nm. Blood was retrieved retroorbitally and also imaged to measure fluorescence intensities. Background fluorescence (PBS group) was subtracted. To estimate the starting concentration of PBs in the blood (t = 0), each 50 μL of blood, which corresponds to about 1:30 of the total blood volume of a mouse of the age used in this study by us, of two different mice was mixed with a 1:30 ratio of the respective PB formulations applied *in vivo*, and fluorescence levels were measured (PBs: 7664 ± 0.3098, PB−aDEC205[2]: 5784 ± 1399, PB−aDEC205[6]: 6752 ± 2167, PB−aDEC205[12]: 6624 ± 1090). Mice were sacrificed at the indicated time points, and organs (liver, heart, lungs, spleen, and inguinal as well as popliteal LNs) were dissected and imaged as above. Fluorescence intensities are presented as total radiant efficiency ([p/s]/[μW/cm^2]).

Separation by Asymmetrical Flow Field-Flow Fractionation (AF4). The AF4 measurements were performed using an installation from the ConSenxuS GmbH. The setup was composed of a constaMETRICR 3200 main pump and a Spectra Series UV150 detector from Thermos Separation, a Dark V3 LS detector from ConSenxuS GmbH, a Pharmacia P-3500 injection pump, an LV-F flow controller from Horiba ATEC, a Waters in-line degasser-AF, and a separation channel with a 190 μm spacer and a regenerated cellulose membrane with a molecular weight cutoff of 10 kDa. The UV

https://doi.org/10.1021/acsnano.1c05713
ACS Nano 2021, 15, 15191−15209

absorption of PBs was detected at 220 nm. For all measurements, phosphate-buffered saline (151.7×10^{-3} m) was used as solvent; it also contained sodium azide in a concentration of 0.2×10^{-3} m. The main flow was 1 mL min^{-1} higher than the cross-flow for each measurement. The cross-flow is illustrated in the AF4 elugram (see Supp Figure 5). Every measurement was carried out at least three times from three independent incubation experiments. PB fractions were collected from 13.3 to 18.3 min. To increase the concentration of the collected fractions from the AF4 after the separation process, they were filtrated with Amikon Ultra centrifugal filters from Merck Millipore with a regenerated cellulose membrane and a molecular weight cutoff of 3 kDa. Plasma and particle controls were performed as described.[24]

SDS-PAGE. SDS-PAGE experiments were performed following the general protocol of Laemmli. The polyacrylamide gels were composed of a 12% separation gel (with 8% stacking gel), and the electrophoresis was carried out for 45 min at 200 V with a Mini-PROTEAN Tetra Vertical electrophoresis chamber from BIO-RAD. A 7.5 μL amount of each sample was incubated with 2.5 μL of loading buffer (NuPAGE LDS sample buffer, Invitrogen) for 5 min at 95 °C. Novex Sharp pre-stained protein standard from Invitrogen was loaded on each gel as a protein ladder for comparison. The proteins in the gels were visualized using silver staining.

Dynamic Light Scattering. For DLS experiments the collected fractions from the AF4 were prepared in a dust-free flow-box. They were filtered with syringe filters from PALL Life Science with a diameter of 13 mm and a GHP membrane (0.2 μm pores) into dust-free cylindrical scattering cells (Suprasil, 20 mm diameter). The measurements were performed with a Uniphase He/Ne laser (632.8 nm, 22 mW), an ALV-SP125 goniometer, an ALV/High QE APD-Avalanche photodiode, an ALV5000/E/PCI correlator, and a Lauda RC-6 thermostat unit. All angular-dependent measurements were carried out in 20° steps between 30° and 150°. Data analysis was performed according to the procedure described by Rausch and co-workers.[76]

Protein Digestion. Lyophilized protein corona proteins were digested according to the SP3 ("single-pot solid-phase-enhanced sample preparation") protocol.[77] After solubilization in SDS-Lysis buffer (1% SDS, 1× complete Protease Inhibitor Cocktail-EDTA, 50 mM HEPES, pH 8,5), proteins were reduced by adding 5 μL of 200 mM dithiothreitol (DTT) per 100 μL of lysate (45 °C, 30 min). Free cysteines were subsequently alkylated by adding 10 μL of 100 mM iodoacetamide (IAA) per 100 μL of lysate (RT, 30 min, in the dark). Subsequently, the remaining IAA was quenched by adding 10 μL of 200 mM DTT per 100 μL of lysate. Magnetic carboxylate-modified particle beads (SpeedBeads, Sigma) were used for protein clean-up, and acetonitrile (ACN), in a final concentration of 70%, was added to the samples to induce the binding of the proteins to the beads by hydrophilic interactions (RT, 18 min). By incubating the bead–protein mixture on a magnetic stand for 2 min, the sample was bound to the magnet and the supernatant was removed, followed by two washing steps with 70% ethanol (EtOH), addition of 180 μL of ACN, incubation for 15 s, and removal of the solvent. Finally, 5 μL of digestion buffer (50 mM ammonium bicarbonate, 1:25 w/w trypsin:protein ratio) was added to the air-dried bead–protein mixtures and incubated overnight at 37 °C. To purify peptides after digestion, ACN was added to a final concentration of 95%. After another washing step (see Sielaff *et al.*, 2017, for detailed information) the beads were resuspended in 10 μL of 2% DMSO (in water), put into an ultrasonic bath for 1 min, and then shortly centrifuged. A 10 μL portion of the resulting supernatant was mixed with 5 μL of 100 fmol/μL Enolase digest (Waters, Eschborn, Germany) and acidified with 5 μL of 1% formic acid (FA).

Liquid Chromatography–Mass Spectroscopy (LC-MS). LC analysis of tryptic peptides was performed on a NanoAQUITY UPLC system (Waters Corporation, Milford, MA, USA) equipped with 75 μM × 250 mm HSS-T3 C18 column (Waters Corporation). Mobile phase A was 0.1% (v/v) FA and 3% (v/v) DMSO in water. Mobile phase B was 0.1% (v/v) FA and 3% (v/v) DMSO in ACN. Peptides were separated running a gradient from 5% to 60% (v/v) mobile phase B at a flow rate of 300 nL/min over 60 min. The column was heated to 55 °C. MS analysis of eluting peptides was performed by data-independent acquisition in MS^E. In brief, precursor ion information was collected in low-energy MS mode at a constant collision energy of 4 eV. Fragment ion information was obtained in the elevated energy scan applying drift-time-specific collision energies. The spectral acquisition time in each mode was 0.6 s with a 0.05 s interscan delay, resulting in an overall cycle time of 1.3 s for the acquisition of one cycle of low and elevated energy data. [Glu1]-fibrinopeptide was used as lock mass at 100 fmol/μL and sampled every 30 s into the mass spectrometer *via* the reference sprayer of the NanoLockSpray source. All samples were analyzed in three technical replicates.

Data Processing and Label-Free Quantification. MS^E data processing and database search were performed using ProteinLynx Global Server (PLGS, ver. 3.0.2, Waters Corporation). The resulting proteins were searched in the UniProt human proteome database (UniProtKB release 2017_05, 20,201 entries)[78] supplemented with a list of common contaminants. The database search was specified by trypsin as enzyme for digestion, and peptides with up to two missed cleavages were included. Furthermore, carbamidomethyl cysteine was set as fixed modification and oxidized methionine as variable modification. False discovery rate assessment for peptide and protein identification was done using the target-decoy strategy by searching a reverse database and was set to 0.01 for database search in PLGS. Retention time alignment, exact mass retention time, normalization, and filtering was performed in ISOQuant ver.1.8.[79] By using TOP3 quantification,[80] absolute in-sample amounts of proteins were calculated. Statistical analysis was done in Perseus,[81] by performing two-tailed, paired tests and subsequent Benjamini–Hochberg correction.[82] Q-values < 0.05 were considered significant.

ASSOCIATED CONTENT

Supporting Information

The Supporting Information is available free of charge at https://pubs.acs.org/doi/10.1021/acsnano.1c05713.

Binding of PB derivatives to liver cell populations, effects of FcR blockade on binding to liver cell populations, LN and spleen DC populations (PDF)

AUTHOR INFORMATION

Corresponding Authors

Matthias Bros − *Department of Dermatology, University Medical Center of the Johannes Gutenberg University Mainz, 55131 Mainz, Germany*; Email: mbros@uni-mainz.de

Stephan Grabbe − *Department of Dermatology, University Medical Center of the Johannes Gutenberg University Mainz, 55131 Mainz, Germany*; Email: stephan.grabbe@unimedizin-mainz.de

Matthias Barz − *Leiden Academic Center for Drug Research (LACDR), Leiden University, 2333 CC Leiden, The Netherlands; Department of Chemistry, Johannes Gutenberg University, 55099 Mainz, Germany; Department of Dermatology, University Medical Center of the Johannes Gutenberg University Mainz, 55131 Mainz, Germany;* orcid.org/0000-0002-1749-9034; Email: mbarz@lacdr.leidenuniv.nl

Authors

Cinja Kappel − *Department of Dermatology, University Medical Center of the Johannes Gutenberg University Mainz, 55131 Mainz, Germany;* orcid.org/0000-0002-9122-0601

Christine Seidl − *Department of Chemistry, Johannes Gutenberg University, 55099 Mainz, Germany; Leiden*

Academic Center for Drug Research (LACDR), Leiden University, 2333 CC Leiden, The Netherlands
Carolina Medina-Montano − *Department of Dermatology, University Medical Center of the Johannes Gutenberg University Mainz, 55131 Mainz, Germany*
Meike Schinnerer − *Department of Chemistry, Johannes Gutenberg University, 55099 Mainz, Germany*
Irina Alberg − *Department of Chemistry, Johannes Gutenberg University, 55099 Mainz, Germany*
Christian Leps − *Institute for Immunology, University Medical Center of the Johannes Gutenberg University Mainz, 55131 Mainz, Germany*
Julian Sohl − *Institute for Immunology, University Medical Center of the Johannes Gutenberg University Mainz, 55131 Mainz, Germany*
Ann-Kathrin Hartmann − *Institute for Immunology, University Medical Center of the Johannes Gutenberg University Mainz, 55131 Mainz, Germany*
Michael Fichter − *Department of Dermatology, University Medical Center of the Johannes Gutenberg University Mainz, 55131 Mainz, Germany*
Michael Kuske − *Department of Dermatology, University Medical Center of the Johannes Gutenberg University Mainz, 55131 Mainz, Germany*
Jenny Schunke − *Department of Dermatology, University Medical Center of the Johannes Gutenberg University Mainz, 55131 Mainz, Germany*
Gabor Kuhn − *Department of Dermatology, University Medical Center of the Johannes Gutenberg University Mainz, 55131 Mainz, Germany*
Ingrid Tubbe − *Department of Dermatology, University Medical Center of the Johannes Gutenberg University Mainz, 55131 Mainz, Germany*
David Paßlick − *Department of Dermatology, University Medical Center of the Johannes Gutenberg University Mainz, 55131 Mainz, Germany*
Dominika Hobernik − *Department of Dermatology, University Medical Center of the Johannes Gutenberg University Mainz, 55131 Mainz, Germany*
Rebekka Bent − *Department of Dermatology, University Medical Center of the Johannes Gutenberg University Mainz, 55131 Mainz, Germany*
Katharina Haas − *Department of Dermatology, University Medical Center of the Johannes Gutenberg University Mainz, 55131 Mainz, Germany*
Evelyn Montermann − *Department of Dermatology, University Medical Center of the Johannes Gutenberg University Mainz, 55131 Mainz, Germany*
Kerstin Walzer − *TRON−Translational Oncology at the University Medical Center of the Johannes Gutenberg University GmbH, 55131 Mainz, Germany*
Mustafa Diken − *TRON−Translational Oncology at the University Medical Center of the Johannes Gutenberg University GmbH, 55131 Mainz, Germany; Biontech AG, 55131 Mainz, Germany*
Manfred Schmidt − *Institute for Physical Chemistry, Johannes Gutenberg University, 55099 Mainz, Germany*
Rudolf Zentel − *Department of Chemistry, Johannes Gutenberg University, 55099 Mainz, Germany;* orcid.org/0000-0001-9206-6047
Lutz Nuhn − *Max Planck Institute for Polymer Research, 55128 Mainz, Germany;* orcid.org/0000-0003-0761-1106
Hansjörg Schild − *Institute for Immunology, University Medical Center of the Johannes Gutenberg University Mainz, 55131 Mainz, Germany*
Stefan Tenzer − *Institute for Immunology, University Medical Center of the Johannes Gutenberg University Mainz, 55131 Mainz, Germany;* orcid.org/0000-0003-3034-0017
Volker Mailänder − *Department of Dermatology, University Medical Center of the Johannes Gutenberg University Mainz, 55131 Mainz, Germany;* orcid.org/0000-0001-6583-8136

Complete contact information is available at: https://pubs.acs.org/10.1021/acsnano.1c05713

Author Contributions

C. Kappel and C. Medina-Montano performed the *in vitro* and *in vivo* studies. C. Seidl and M. Schinnerer synthesized and characterized the polymer brushes and corresponding conjugates, etc. M. Fichter, M. Kuske, J. Schunke, G. Kuhn, I. Tubbe, D. Paßlick, D. Hobernik, R. Bent, K. Haas, E. Montermann, J. Sohl, and A.-K. Hartmann assisted during or performed the *in vivo* studies. M. Diken and K. Walzer conducted the biodistribution studies. C. Leps and I. Alberg conducted and Stefan Tenzer supervised the mass spectroscopy studies on protein corona formation. V. Mailänder contributed to the planning of the *in vivo* studies and the discussion of the results. M. Schmidt, R. Zentel, L. Nuhn, and H. Schild contributed to evaluation of data and contributed to the discussion of results. The project was designed and supervised by M. Barz, M. Bros, and S. Grabbe.

Notes

The authors declare no competing financial interest.

ACKNOWLEDGMENTS

This work was funded by the Deutsche Forschungsgemeinschaft (DFG, German Research Foundation) SFB-Geschäftszeichen SFB 1066/3 2021 213555243; TP B4, TP A6, Q6. We would like to thank S. Gehring and co-workers for their support, as well as the Institute of Molecular Biology (IMB, Mainz Germany). We also thank C. Rosenauer (Morsbach lab, Max Planck Institute for Polymer Research, Mainz, Germany) for performing DLS measurements.

REFERENCES

(1) Kulshrestha, S.; Khan, A. U. Nanomedicine for Anticancer and Antimicrobial Treatment: An Overview. *IET Nanobiotechnol.* **2018**, *12* (8), 1009−1017.
(2) Ajorlou, E.; Khosroushahi, A. Y. Trends on Polymer- and Lipid-Based Nanostructures for Parenteral Drug Delivery to Tumors. *Cancer Chemother. Pharmacol.* **2017**, *79* (2), 251−265.
(3) Maeda, H.; Nakamura, H.; Fang, J. The EPR Effect for Macromolecular Drug Delivery to Solid Tumors: Improvement of Tumor Uptake, Lowering of Systemic Toxicity, and Distinct Tumor Imaging *in Vivo*. *Adv. Drug Delivery Rev.* **2013**, *65* (1), 71−9.
(4) Huang, P.; Wang, X.; Liang, X.; Yang, J.; Zhang, C.; Kong, D.; Wang, W. Nano-, Micro-, and Macroscale Drug Delivery Systems for Cancer Immunotherapy. *Acta Biomater.* **2019**, *85*, 1−26.
(5) Kelly, H. G.; Kent, S. J.; Wheatley, A. K. Immunological Basis for Enhanced Immunity of Nanoparticle Vaccines. *Expert Rev. Vaccines* **2019**, *18* (3), 269−280.
(6) Grabbe, S.; Landfester, K.; Schuppan, D.; Barz, M.; Zentel, R. Nanoparticles and the Immune System: Challenges and Opportunities. *Nanomedicine (London, U. K.)* **2016**, *11* (20), 2621−2624.
(7) Lee, G.; Han, S.; Inocencio, I.; Cao, E.; Hong, J.; Phillips, A. R. J.; Windsor, J. A.; Porter, C. J. H.; Trevaskis, N. L. Lymphatic Uptake

of Liposomes after Intraperitoneal Administration Primarily Occurs *via* the Diaphragmatic Lymphatics and Is Dependent on Liposome Surface Properties. *Mol. Pharmaceutics* **2019**, *16* (12), 4987−4999.
(8) Germic, N.; Frangez, Z.; Yousefi, S.; Simon, H. U. Regulation of the Innate Immune System by Autophagy: Monocytes, Macrophages, Dendritic Cells and Antigen Presentation. *Cell Death Differ.* **2019**, *26* (4), 715−727.
(9) Shen, L.; Tenzer, S.; Storck, W.; Hobernik, D.; Raker, V. K.; Fischer, K.; Decker, S.; Dzionek, A.; Krauthauser, S.; Diken, M.; Nikolaev, A.; Maxeiner, J.; Schuster, P.; Kappel, C.; Verschoor, A.; Schild, H.; Grabbe, S.; Bros, M. Protein Corona-Mediated Targeting of Nanocarriers to B Cells Allows Redirection of Allergic Immune Responses. *J. Allergy Clin. Immunol.* **2018**, *142* (5), 1558−1570.
(10) Bros, M.; Nuhn, L.; Simon, J.; Moll, L.; Mailander, V.; Landfester, K.; Grabbe, S. The Protein Corona as a Confounding Variable of Nanoparticle-Mediated Targeted Vaccine Delivery. *Front. Immunol.* **2018**, *9*, 1760.
(11) Hey, Y. Y.; O'Neill, H. C. Murine Spleen Contains a Diversity of Myeloid and Dendritic Cells Distinct in Antigen Presenting Function. *Journal of Cellular and Molecular Medicine* **2012**, *16* (11), 2611−9.
(12) Tran, T. H.; Tran, T. T. P.; Nguyen, H. T.; Phung, C. D.; Jeong, J. H.; Stenzel, M. H.; Jin, S. G.; Yong, C. S.; Truong, D. H.; Kim, J. O. Nanoparticles for Dendritic Cell-Based Immunotherapy. *Int. J. Pharm.* **2018**, *542* (1−2), 253−265.
(13) Tjandra, K. C.; Thordarson, P. Multivalency in Drug Delivery-When Is It Too Much of a Good Thing? *Bioconjugate Chem.* **2019**, *30* (3), 503−514.
(14) Zern, B. J.; Chacko, A. M.; Liu, J.; Greineder, C. F.; Blankemeyer, E. R.; Radhakrishnan, R.; Muzykantov, V. Reduction of Nanoparticle Avidity Enhances the Selectivity of Vascular Targeting and PET Detection of Pulmonary Inflammation. *ACS Nano* **2013**, *7* (3), 2461−9.
(15) Sondermann, P.; Szymkowski, D. E. Harnessing Fc Receptor Biology in the Design of Therapeutic Antibodies. *Curr. Opin. Immunol.* **2016**, *40*, 78−87.
(16) Alkilany, A. M.; Zhu, L.; Weller, H.; Mews, A.; Parak, W. J.; Barz, M.; Feliu, N. Ligand Density on Nanoparticles: A Parameter with Critical Impact on Nanomedicine. *Adv. Drug Delivery Rev.* **2019**, *143*, 22−36.
(17) Faria, M.; Bjornmalm, M.; Thurecht, K. J.; Kent, S. J.; Parton, R. G.; Kavallaris, M.; Johnston, A. P. R.; Gooding, J. J.; Corrie, S. R.; Boyd, B. J.; Thordarson, P.; Whittaker, A. K.; Stevens, M. M.; Prestidge, C. A.; Porter, C. J. H.; Parak, W. J.; Davis, T. P.; Crampin, E. J.; Caruso, F. Minimum Information Reporting in Bio-Nano Experimental Literature. *Nat. Nanotechnol.* **2018**, *13* (9), 777−785.
(18) Buhler, J.; Gietzen, S.; Reuter, A.; Kappel, C.; Fischer, K.; Decker, S.; Schaffel, D.; Koynov, K.; Bros, M.; Tubbe, I.; Grabbe, S.; Schmidt, M. Selective Uptake of Cylindrical Poly(2-Oxazoline) Brush-AntiDEC205 Antibody-OVA Antigen Conjugates into DEC-Positive Dendritic Cells and Subsequent T-Cell Activation. *Chem. - Eur. J.* **2014**, *20* (39), 12405−10.
(19) Bargheer, D.; Giemsa, A.; Freund, B.; Heine, M.; Waurisch, C.; Stachowski, G. M.; Hickey, S. G.; Eychmuller, A.; Heeren, J.; Nielsen, P. The Distribution and Degradation of Radiolabeled Superparamagnetic Iron Oxide Nanoparticles and Quantum Dots in Mice. *Beilstein J. Nanotechnol.* **2015**, *6*, 111−123.
(20) Shen, L.; Krauthauser, S.; Fischer, K.; Hobernik, D.; Abassi, Y.; Dzionek, A.; Nikolaev, A.; Voltz, N.; Diken, M.; Krummen, M.; Montermann, E.; Tubbe, I.; Lorenz, S.; Strand, D.; Schild, H.; Grabbe, S.; Bros, M. Vaccination with Trifunctional Nanoparticles that Address CD8(+) Dendritic Cells Inhibits Growth of Established Melanoma. *Nanomedicine (London, U. K.)* **2016**, *11* (20), 2647−2662.
(21) Birke, A.; Huesmann, D.; Kelsch, A.; Weilbacher, M.; Xie, J.; Bros, M.; Bopp, T.; Becker, C.; Landfester, K.; Barz, M. Polypeptoid-Block-Polypeptide Copolymers: Synthesis, Characterization, and Application of Amphiphilic Block Copolypept(o)ides in Drug Formulations and Miniemulsion Techniques. *Biomacromolecules* **2014**, *15* (2), 548−57.
(22) Birke, A.; Ling, J.; Barz, M. Polysarcosine-Containing Copolymers: Synthesis, Characterization, Self-Assembly, and Applications. *Prog. Polym. Sci.* **2018**, *81*, 163−208.
(23) Fenaroli, F.; Repnik, U.; Xu, Y.; Johann, K.; Van Herck, S.; Dey, P.; Skjeldal, F. M.; Frei, D. M.; Bagherifam, S.; Kocere, A.; Haag, R.; De Geest, B. G.; Barz, M.; Russell, D. G.; Griffiths, G. Enhanced Permeability and Retention-Like Extravasation of Nanoparticles from the Vasculature into Tuberculosis Granulomas in Zebrafish and Mouse Models. *ACS Nano* **2018**, *12* (8), 8646−8661.
(24) Alberg, I.; Kramer, S.; Schinnerer, M.; Hu, Q.; Seidl, C.; Leps, C.; Drude, N.; Mockel, D.; Rijcken, C.; Lammers, T.; Diken, M.; Maskos, M.; Morsbach, S.; Landfester, K.; Tenzer, S.; Barz, M.; Zentel, R. Polymeric Nanoparticles with Neglectable Protein Corona. *Small* **2020**, *16* (18), No. e1907574.
(25) Bonifaz, L. C.; Bonnyay, D. P.; Charalambous, A.; Darguste, D. I.; Fujii, S.; Soares, H.; Brimnes, M. K.; Moltedo, B.; Moran, T. M.; Steinman, R. M. *In vivo* Targeting of Antigens to Maturing Dendritic Cells *via* The DEC-205 Receptor Improves T Cell Vaccination. *J. Exp. Med.* **2004**, *199* (6), 815−24.
(26) Hörtz, C.; Birke, A.; Kaps, L.; Decker, S.; Wächtersbach, E.; Fischer, K.; Schuppan, D.; Barz, M.; Schmidt, M. Cylindrical Brush Polymers with Polysarcosine Side Chains: A Novel Biocompatible Carrier for Biomedical Applications. *Macromolecules* **2015**, *48* (7), 2074−2086.
(27) Ulbricht, J.; Jordan, R.; Luxenhofer, R. On the Biodegradability of Polyethylene Glycol, Polypeptoids and Poly(2-Oxazoline)s. *Biomaterials* **2014**, *35* (17), 4848−61.
(28) Dal, N. K.; Kocere, A.; Wohlmann, J.; Van Herck, S.; Bauer, T. A.; Resseguier, J.; Bagherifam, S.; Hyldmo, H.; Barz, M.; De Geest, B. G.; Fenaroli, F. Zebrafish Embryos Allow Prediction of Nanoparticle Circulation Times in Mice and Facilitate Quantification of Nanoparticle-Cell Interactions. *Small* **2020**, *16* (5), No. e1906719.
(29) Shortman, K.; Heath, W. R. The CD8+ Dendritic Cell Subset. *Immunol. Rev.* **2010**, *234* (1), 18−31.
(30) Yi, G.; Son, J.; Yoo, J.; Park, C.; Koo, H. Application of Click Chemistry in Nanoparticle Modification and Its Targeted Delivery. *Biomaterials Research* **2018**, *22*, 13.
(31) Sadauskas, E.; Wallin, H.; Stoltenberg, M.; Vogel, U.; Doering, P.; Larsen, A.; Danscher, G. Kupffer Cells Are Central in the Removal of Nanoparticles from the Organism. *Part. Fibre Toxicol.* **2007**, *4*, 10.
(32) Zhang, Y. N.; Poon, W.; Tavares, A. J.; McGilvray, I. D.; Chan, W. C. W. Nanoparticle-Liver Interactions: Cellular Uptake and Hepatobiliary Elimination. *J. Controlled Release* **2016**, *240*, 332−348.
(33) Scott, C. L.; Zheng, F.; De Baetselier, P.; Martens, L.; Saeys, Y.; De Prijck, S.; Lippens, S.; Abels, C.; Schoonooghe, S.; Raes, G.; Devoogdt, N.; Lambrecht, B. N.; Beschin, A.; Guilliams, M. Bone Marrow-Derived Monocytes Give Rise to Self-Renewing and Fully Differentiated Kupffer Cells. *Nat. Commun.* **2016**, *7*, 10321.
(34) Jenne, C. N.; Kubes, P. Immune Surveillance by the Liver. *Nat. Immunol.* **2013**, *14* (10), 996−1006.
(35) Ganesan, L. P.; Kim, J.; Wu, Y.; Mohanty, S.; Phillips, G. S.; Birmingham, D. J.; Robinson, J. M.; Anderson, C. L. FcgammaRIIb on Liver Sinusoidal Endothelium Clears Small Immune Complexes. *J. Immunol.* **2012**, *189* (10), 4981−8.
(36) Anania, J. C.; Chenoweth, A. M.; Wines, B. D.; Hogarth, P. M. The Human FcgammaRII (CD32) Family of Leukocyte FcR in Health and Disease. *Front. Immunol.* **2019**, *10*, 464.
(37) Kurlander, R. J.; Ellison, D. M.; Hall, J. The Blockade of Fc Receptor-Mediated Clearance of Immune Complexes *in Vivo* by a Monoclonal Antibody (2.4G2) Directed against Fc Receptors on Murine Leukocytes. *J. Immunol.* **1984**, *133* (2), 855−862.
(38) Vidarsson, G.; Dekkers, G.; Rispens, T. IgG Subclasses and Allotypes: From Structure to Effector Functions. *Front. Immunol.* **2014**, *5*, 520.
(39) Dzik, S. Complement and Coagulation: Cross Talk through Time. *Transfusion Medicine Reviews* **2019**, *33* (4), 199−206.
(40) Andrew, S. M.; Titus, J. A., Fragmentation of Immunoglobulin G. *Curr. Protoc Cell Biol.* 2003, Chapter 16, Unit 16.4.

https://doi.org/10.1021/acsnano.1c05713
ACS Nano 2021, 15, 15191−15209

(41) De Jong, W. H.; Hagens, W. I.; Krystek, P.; Burger, M. C.; Sips, A. J.; Geertsma, R. E. Particle Size-Dependent Organ Distribution of Gold Nanoparticles after Intravenous Administration. *Biomaterials* **2008**, *29* (12), 1912−9.
(42) Chattopadhyay, N.; Fonge, H.; Cai, Z.; Scollard, D.; Lechtman, E.; Done, S. J.; Pignol, J. P.; Reilly, R. M. Role of Antibody-Mediated Tumor Targeting and Route of Administration in Nanoparticle Tumor Accumulation *in Vivo*. *Mol. Pharmaceutics* **2012**, *9* (8), 2168−79.
(43) Jain, N.; Smith, S. W.; Ghone, S.; Tomczuk, B. Current ADC Linker Chemistry. *Pharm. Res.* **2015**, *32* (11), 3526−40.
(44) Yang, Y.; Mu, J.; Xing, B. Photoactivated Drug Delivery and Bioimaging. *Wiley Interdisciplinary Reviews. Nanomedicine and Nanobiotechnology* **2017**, *9* (2), 1−19.
(45) Nessler, I.; Cilliers, C.; Thurber, G. M. Practical Guide for Quantification of *in Vivo* Degradation Rates for Therapeutic Proteins with Single-Cell Resolution Using Fluorescence Ratio Imaging. *Pharmaceutics* **2020**, *12* (2), 1−13.
(46) Yu, S. S. Evaluating Nanoparticle Binding to Blood Compartment Immune Cells in High-Throughput with Flow Cytometry. *Methods Mol. Biol. (N. Y., NY, U. S.)* **2017**, *1570*, 139−153.
(47) Samuelsson, E.; Shen, H.; Blanco, E.; Ferrari, M.; Wolfram, J. Contribution of Kupffer Cells to Liposome Accumulation in the Liver. *Colloids Surf., B* **2017**, *158*, 356−362.
(48) Park, J. K.; Utsumi, T.; Seo, Y. E.; Deng, Y.; Satoh, A.; Saltzman, W. M.; Iwakiri, Y. Cellular Distribution of Injected PLGA-Nanoparticles in the Liver. *Nanomedicine* **2016**, *12* (5), 1365−74.
(49) Malovic, I.; Sorensen, K. K.; Elvevold, K. H.; Nedredal, G. I.; Paulsen, S.; Erofeev, A. V.; Smedsrod, B. H.; McCourt, P. A. The Mannose Receptor on Murine Liver Sinusoidal Endothelial Cells Is the Main Denatured Collagen Clearance Receptor. *Hepatology (Hoboken, NJ, U. S.)* **2007**, *45* (6), 1454−61.
(50) Seckert, C. K.; Renzaho, A.; Tervo, H. M.; Krause, C.; Deegen, P.; Kuhnapfel, B.; Reddehase, M. J.; Grzimek, N. K. Liver Sinusoidal Endothelial Cells Are a Site of Murine Cytomegalovirus Latency and Reactivation. *J. Virol.* **2009**, *83* (17), 8869−84.
(51) Oie, C. I.; Appa, R. S.; Hilden, I.; Petersen, H. H.; Gruhler, A.; Smedsrod, B.; Hansen, J. B. Rat Liver Sinusoidal Endothelial Cells (LSECs) Express Functional Low Density Lipoprotein Receptor-Related Protein-1 (LRP-1). *J. Hepatol.* **2011**, *55* (6), 1346−52.
(52) Ganesan, L. P.; Mates, J. M.; Cheplowitz, A. M.; Avila, C. L.; Zimmerer, J. M.; Yao, Z.; Maiseyeu, A.; Rajaram, M. V.; Robinson, J. M.; Anderson, C. L. Scavenger Receptor B1, the HDL Receptor, Is Expressed Abundantly in Liver Sinusoidal Endothelial Cells. *Sci. Rep.* **2016**, *6*, 20646.
(53) Hayashi, Y.; Takamiya, M.; Jensen, P. B.; Ojea-Jiménez, I.; Claude, H.; Antony, C.; Kjaer-Sorensen, K.; Grabher, C.; Boesen, T.; Gilliland, D.; Oxvig, C.; Strähle, U.; Weiss, C. Differential Nanoparticle Sequestration by Macrophages and Scavenger Endothelial Cells Visualized *in Vivo* in Real-Time and at Ultrastructural Resolution. *ACS Nano* **2020**, *14* (2), 1665−1681.
(54) Mates, J. M.; Yao, Z.; Cheplowitz, A. M.; Suer, O.; Phillips, G. S.; Kwiek, J. J.; Rajaram, M. V.; Kim, J.; Robinson, J. M.; Ganesan, L. P.; Anderson, C. L. Mouse Liver Sinusoidal Endothelium Eliminates HIV-Like Particles from Blood at a Rate of 100 Million per Minute by a Second-Order Kinetic Process. *Front. Immunol.* **2017**, *8*, 35.
(55) Cheng, W. W.; Allen, T. M. Targeted Delivery of Anti-CD19 Liposomal Doxorubicin in B-cell Lymphoma: A Comparison of Whole Monoclonal Antibody, Fab' Fragments and Single Chain Fv. *J. Controlled Release* **2008**, *126* (1), 50−8.
(56) Chaubey, P.; Mishra, B. Mannose-Conjugated Chitosan Nanoparticles Loaded with Rifampicin for the Treatment of Visceral Leishmaniasis. *Carbohydr. Polym.* **2014**, *101*, 1101−8.
(57) Higuchi, Y.; Nishikawa, M.; Kawakami, S.; Yamashita, F.; Hashida, M. Uptake Characteristics of Mannosylated and Fucosylated Bovine Serum Albumin in Primary Cultured Rat Sinusoidal Endothelial Cells and Kupffer Cells. *Int. J. Pharm.* **2004**, *287* (1−2), 147−54.
(58) Armengol, C.; Bartoli, R.; Sanjurjo, L.; Serra, I.; Amezaga, N.; Sala, M.; Sarrias, M. R. Role of Scavenger Receptors in the Pathophysiology of Chronic Liver Diseases. *Crit. Rev. Immunol.* **2013**, *33* (1), 57−96.
(59) Zhou, H.; Fan, Z.; Li, P. Y.; Deng, J.; Arhontoulis, D. C.; Li, C. Y.; Bowne, W. B.; Cheng, H. Dense and Dynamic Polyethylene Glycol Shells Cloak Nanoparticles from Uptake by Liver Endothelial Cells for Long Blood Circulation. *ACS Nano* **2018**, *12* (10), 10130−10141.
(60) Sivaram, A. J.; Wardiana, A.; Alcantara, S.; Sonderegger, S. E.; Fletcher, N. L.; Houston, Z. H.; Howard, C. B.; Mahler, S. M.; Alexander, C.; Kent, S. J.; Bell, C. A.; Thurecht, K. J. Controlling the Biological Fate of Micellar Nanoparticles: Balancing Stealth and Targeting. *ACS Nano* **2020**, *14* (10), 13739−13753.
(61) Kohler, H. Natural Antibodies: Next Steps Toward Translational Investigation. *Methods Mol. Biol. (N. Y., NY, U. S.)* **2017**, *1643*, 1−3.
(62) Thurman, J. M.; Panzer, S. E.; Le Quintrec, M. The Role of Complement in Antibody Mediated Transplant Rejection. *Mol. Immunol.* **2019**, *112*, 240−246.
(63) Trevaskis, N. L.; Kaminskas, L. M.; Porter, C. J. From Sewer to Saviour - Targeting the Lymphatic System to Promote Drug Exposure and Activity. *Nat. Rev. Drug Discovery* **2015**, *14* (11), 781−803.
(64) Richards, D. A.; Maruani, A.; Chudasama, V. Antibody Fragments as Nanoparticle Targeting Ligands: A Step in the Right Direction. *Chemical Science* **2017**, *8* (1), 63−77.
(65) Leenheer, D.; Ten Dijke, P.; Hipolito, C. J. A Current Perspective on Applications of Macrocyclic-Peptide-Based High-Affinity Ligands. *Biopolymers* **2016**, *106* (6), 889−900.
(66) Hu, P. P. Recent Advances in Aptamers Targeting Immune System. *Inflammation* **2017**, *40* (1), 295−302.
(67) White, A. L.; Chan, H. T.; Roghanian, A.; French, R. R.; Mockridge, C. I.; Tutt, A. L.; Dixon, S. V.; Ajona, D.; Verbeek, J. S.; Al-Shamkhani, A.; Cragg, M. S.; Beers, S. A.; Glennie, M. J. Interaction with FcgammaRIIB is Critical for the Agonistic Activity of Anti-CD40 Monoclonal Antibody. *J. Immunol.* **2011**, *187* (4), 1754−63.
(68) Kedmi, R.; Veiga, N.; Ramishetti, S.; Goldsmith, M.; Rosenblum, D.; Dammes, N.; Hazan-Halevy, I.; Nahary, L.; Leviatan-Ben-Arye, S.; Harlev, M.; Behlke, M.; Benhar, I.; Lieberman, J.; Peer, D. A Modular Platform for Targeted RNAi Therapeutics. *Nat. Nanotechnol.* **2018**, *13* (3), 214−219.
(69) Tonigold, M.; Simon, J.; Estupinan, D.; Kokkinopoulou, M.; Reinholz, J.; Kintzel, U.; Kaltbeitzel, A.; Renz, P.; Domogalla, M. P.; Steinbrink, K.; Lieberwirth, I.; Crespy, D.; Landfester, K.; Mailander, V. Pre-Adsorption of Antibodies Anables Targeting of Nanocarriers Despite a Biomolecular Corona. *Nat. Nanotechnol.* **2018**, *13* (9), 862−869.
(70) Omstead, D. T.; Mejia, F.; Sjoerdsma, J.; Kim, B.; Shin, J.; Khan, S.; Wu, J.; Kiziltepe, T.; Littlepage, L. E.; Bilgicer, B. *In Vivo* Evaluation of CD38 and CD138 as Targets for Nanoparticle-Based Drug Delivery in Multiple Myeloma. *J. Hematol. Oncol.* **2020**, *13* (1), 145.
(71) Reuter, K. G.; Perry, J. L.; Kim, D.; Luft, J. C.; Liu, R.; DeSimone, J. M. Targeted PRINT Hydrogels: The Role of Nanoparticle Size and Ligand Density on Cell Association, Biodistribution, and Tumor Accumulation. *Nano Lett.* **2015**, *15* (10), 6371−8.
(72) Kranz, L. M.; Diken, M.; Haas, H.; Kreiter, S.; Loquai, C.; Reuter, K. C.; Meng, M.; Fritz, D.; Vascotto, F.; Hefesha, H.; Grunwitz, C.; Vormehr, M.; Hüsemann, Y.; Selmi, A.; Kuhn, A. N.; Buck, J.; Derhovanessian, E.; Rae, R.; Attig, S.; Diekmann, J.; et al. Systemic RNA Delivery to Dendritic Cells Exploits Antiviral Defence for Cancer Immunotherapy. *Nature* **2016**, *534* (7607), 396−401.
(73) Fetsch, C.; Grossmann, A.; Holz, L.; Nawroth, J. F.; Luxenhofer, R. Polypeptoids from *N*-Substituted Glycine *N*-Carboxyanhydrides: Hydrophilic, Hydrophobic, and Amphiphilic Polymers with Poisson Distribution. *Macromolecules* **2011**, *44* (17), 6746−6758.

https://doi.org/10.1021/acsnano.1c05713
ACS Nano 2021, 15, 15191−15209

(74) Gauci, P. J. *Pepsin Digestion of Antibodies to Produce Functional Antigen-Binding Fragments (Fab): A Scientific Fantasy ?/ Penelope J. Gauci and Malcolm R. Alderton*; DSTO Aeronautical and Maritime Research Laboratory: Melbourne, Vic, 2001.
(75) Fichter, M.; Baier, G.; Dedters, M.; Pretsch, L.; Pietrzak-Nguyen, A.; Landfester, K.; Gehring, S. Nanocapsules Generated Out of a Polymeric Dexamethasone Shell Suppress the Inflammatory Response of Liver Macrophages. *Nanomedicine* **2013**, *9* (8), 1223−34.
(76) Rausch, K.; Reuter, A.; Fischer, K.; Schmidt, M. Evaluation of Nanoparticle Aggregation in Human Blood Serum. *Biomacromolecules* **2010**, *11* (11), 2836−9.
(77) Sielaff, M.; Kuharev, J.; Bohn, T.; Hahlbrock, J.; Bopp, T.; Tenzer, S.; Distler, U. Evaluation of FASP, SP3, and iST Protocols for Proteomic Sample Preparation in the Low Microgram Range. *J. Proteome Res.* **2017**, *16* (11), 4060−4072.
(78) UniProt: A Worldwide Wub of Protein Knowledge. *Nucleic Acids Res.* **2019**, *47* (D1), D506−d515.
(79) Distler, U.; Kuharev, J.; Navarro, P.; Tenzer, S. Label-free Quantification in Ion Mobility-Enhanced Data-independent Acquisition Proteomics. *Nat. Protoc.* **2016**, *11* (4), 795−812.
(80) Silva, J. C.; Gorenstein, M. V.; Li, G. Z.; Vissers, J. P.; Geromanos, S. J. Absolute Quantification of Proteins by LCMSE: A Virtue of Parallel MS Acquisition. *Molecular & Cellular Proteomics: MCP* **2006**, *5* (1), 144−56.
(81) Tyanova, S.; Cox, J. Perseus: A Bioinformatics Platform for Integrative Analysis of Proteomics Data in Cancer Research. *Methods Mol. Biol. (N. Y., NY, U. S.)* **2018**, *1711*, 133−148.
(82) Benjamini, Y.; Drai, D.; Elmer, G.; Kafkafi, N.; Golani, I. Controlling the False Discovery Rate in Behavior Genetics Research. *Behav. Brain Res.* **2001**, *125* (1−2), 279−84.

https://doi.org/10.1021/acsnano.1c05713
ACS Nano 2021, 15, 15191−15209